Fast Solvers and Inverse Design Algorithms for Nanophotonic and Radio-Frequency Devices

Constantine Sideris

January 8, 2025

AFOSR EM 2025 PI Review, Dr. Arje Nachman

USC Viterbi School of Engineering

USC University of Southern California

Electromagnetic Device Simulation and Optimization

- Maxwell's equations for EM devices:
  - Nanophotonics
  - Radio-Frequency Devices (antennas, waveguide couplers, passives)

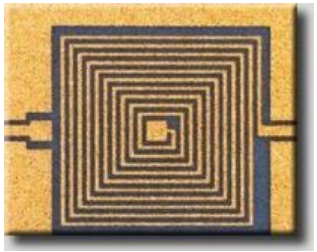

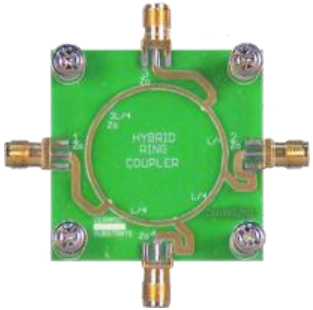

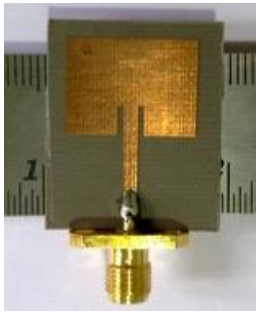

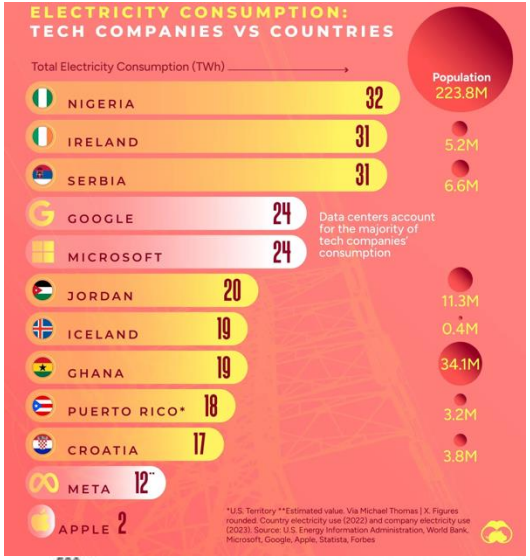

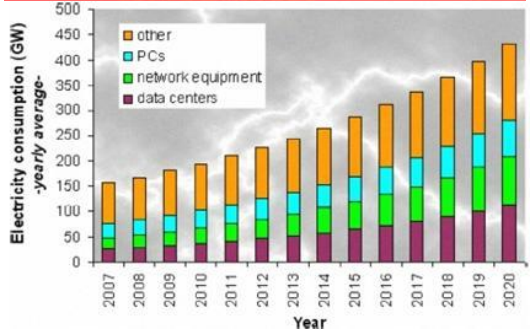

•Analytical solutions: Exist for very few problems
•Optimal design given target metrics usually not intuitive

<u>Increasing networking and communication demands necessitate highly-optimized, energy-efficient technology down to the device level</u>

Outline

1. Introduction
2. **The Multi-Level Interpolated Green Function (IFGF) Method for 3D Maxwell**
3. Corner Regularized Combined Field Integral Equations (CR-CFIE) for Scattering from Objects with Geometric Singularities
4. The Precomputed Numerical Green Function (PNGF) Method for Ultra-fast Inverse Design
   a) Introduction to PNGF
   b) Applications to metallic RF devices
   c) Applications to dielectric nanophotonic devices
5. Conclusions

BIE and High-Order Nyström Methods

- Meshing surfaces vs volumes: O(N^2) unknowns vs O(N^3)
  - Solve for Integral Equation over scattering surface

$$\frac{1}{2}\overline{\varphi}(\boldsymbol{r}) + \int_\Gamma \left(\frac{\partial G(\boldsymbol{r}, \boldsymbol{r}')}{\partial \boldsymbol{n}(\boldsymbol{r}')} - ikG(\boldsymbol{r}, \boldsymbol{r}') \right) \overline{\varphi}(\boldsymbol{r}')\, \mathrm{d}\sigma(\boldsymbol{r}') = -u^{\mathrm{inc}}(\boldsymbol{r}),\ \boldsymbol{r} \in \Gamma$$

- Frequency-domain
  - Dispersion-free
  - Small linear system solved with LU decomposition
  - Iterative methods (e.g. GMRES) for large problems

- Nyström
  - High-order numerical convergence
  - 5 points per wavelength can outperform FDTD at 50 points per wavelength resolution

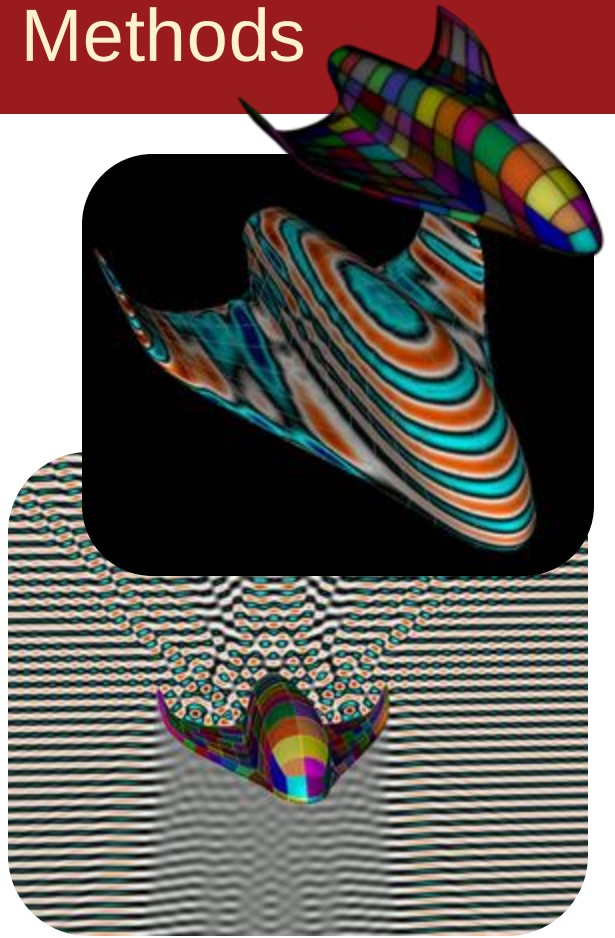

Bruno & Garza, JCP 2020

Chebyshev-Based Boundary Integral Equations (CBIE)

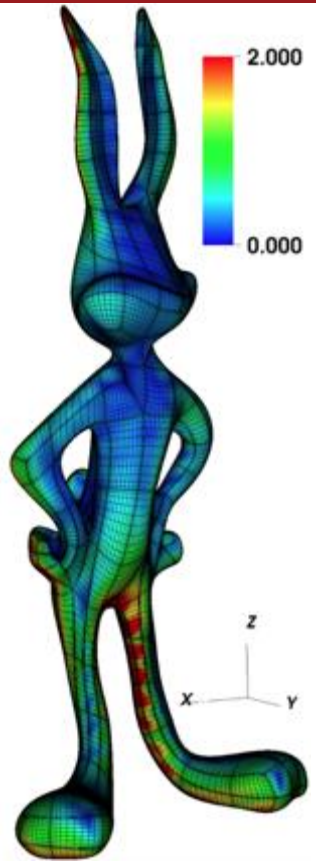

Mesh geometry on Chebyshev grid → Precompute singular integrals → Solve BIE iteratively → Compute fields

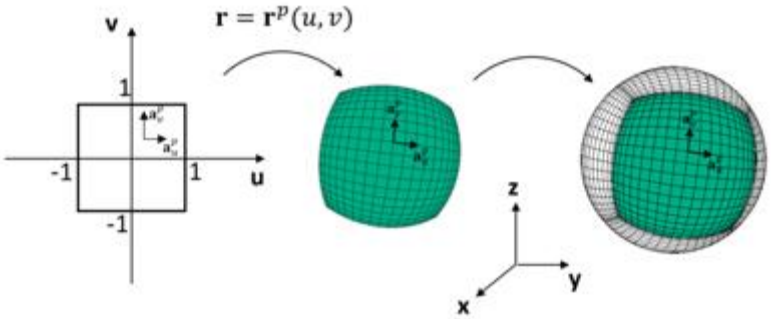

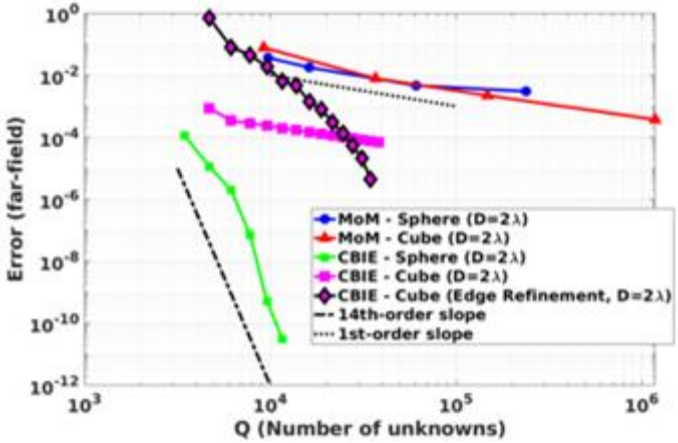

Hu, J., Garza, E., and **Sideris, C.** "A Chebyshev-based high-order-accurate integral equation solver for Maxwell's equations." *IEEE Transactions on Antennas and Propagation* 69.9 (2021): 5790-5800.

Garza, E., Hu, J., and **Sideris, C.** "High-order Chebyshev-based Nyström Methods for Electromagnetics." *2021 International Applied Computational Electromagnetics Society Symposium (ACES)*. IEEE, 2021.

IFGF for Maxwell's Equations

- Unaccelerated BIE methods: $O(N^2)$ time complexity.
- Numerous algorithmic acceleration approaches exist (e.g., FMM, Butterfly, AIM), but they are either specialized for low-frequency problems or require FFTs which are challenging to parallelize.

- Interpolated Factored Green's Function (IFGF) introduced for acoustic scattering in 2021 by Bauinger and Bruno*.
- Single-level IFGF: $O\left(N^{3/2}\right)$, Multi-level IFGF: $O(NlogN)$ time complexity
- Completely FFT free: Parallelizes very easily across many CPUs.
- Simple approach: Interpolate a properly factored Green's function kernel using low-order Chebyshev polynomials.

Paul, J. and **Sideris, C.** "Accelerated 3D Maxwell Integral Equation Solver Using the Interpolated Factored Green Function Method" In revision (IEEE TAP). Available on Arxiv.

IFGF Concept

- Factor out "centered" factor:
- Analytic factor: $\frac{re^{ik(|x-y|-r)}}{|x-y|}$

$$\frac{e^{ik|x-y|}}{|x-y|} = \underbrace{\frac{e^{ikr}}{r}}_{\text{Centered Factor}} \underbrace{\frac{e^{ikr\left(\left|\frac{x-y_c}{r}-\frac{y-y_c}{r}\right|-1\right)}}{\left|\frac{x-y_c}{r}-\frac{y-y_c}{r}\right|}}_{\text{Analytic Factor}}$$

Green function kernel

Slowly oscillating due to factoring out centered factor (easily approximated by polynomial interpolation)

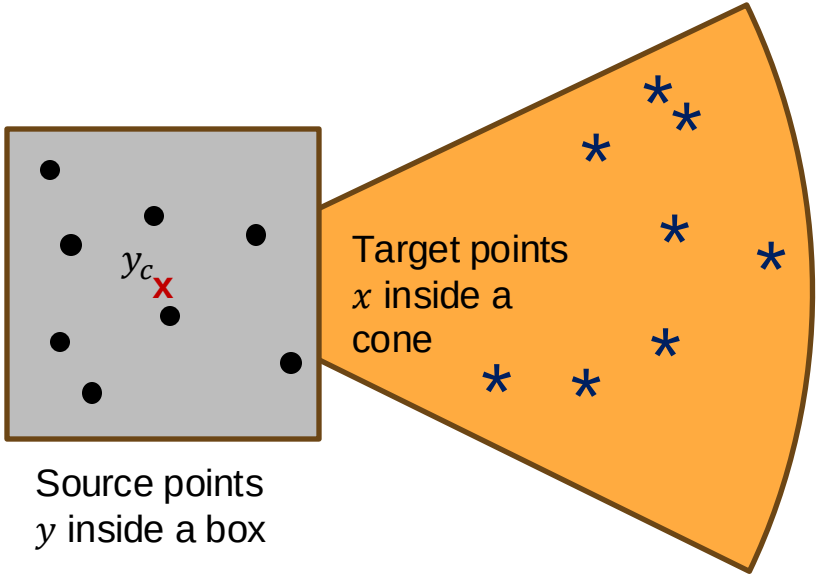

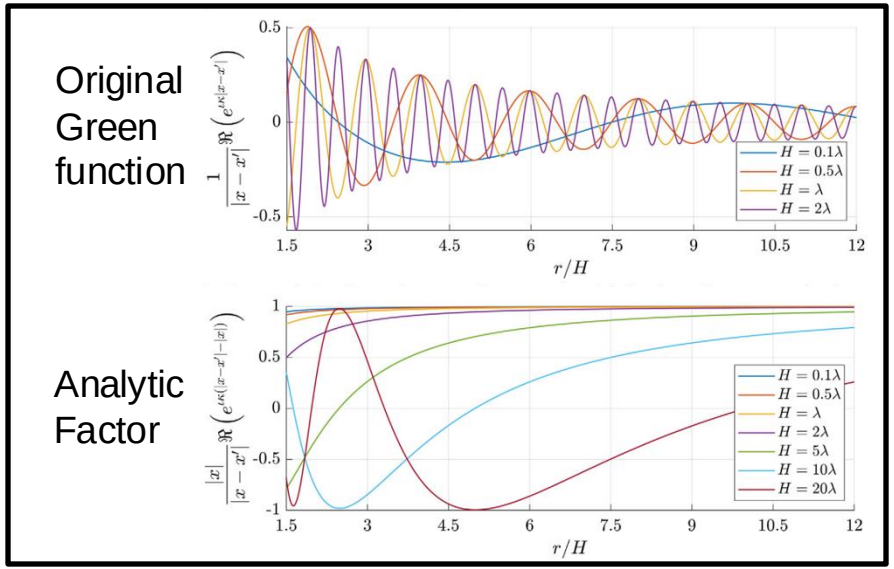

Single-level IFGF Complexity Analysis (Last Year)

- N total points, M boxes, $\frac{N}{M}$ points per box.
- Near interactions cost: $O\left(\frac{N^2}{M}\right)$
- Far interactions cost: $O(MN)$
- Set them equal and solve for optimal M to minimize cost: $MN = \frac{N^2}{M}$
- Optimal $M = \sqrt{N}$
- Resulting asymptotic time complexity: $O\left(N^{\frac{3}{2}}\right)$

Single-level IFGF: PEC Sphere Array (Last Year)

- 17x17x17 array of PEC spheres
- $(\mathrm{D} = 0.125\lambda, \mathrm{spacing} = 0.148\lambda)$
- **5,895,600** unknowns: 4913 spheres * 6 patches per sphere * 10x10 * 2 unknowns per point
- Solved with MFIE: 46 GMRES iterations to reach residual $9\mathrm{x}10^{-4}$
- Total solution time (GPU-IFGF): **656 sec (~11min)**

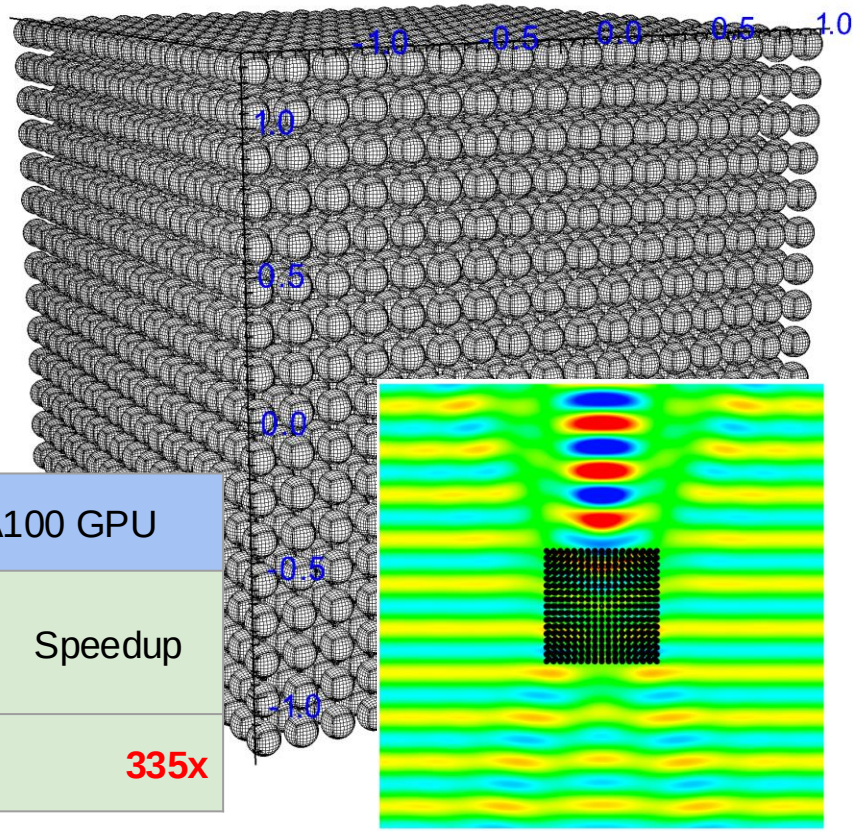

Problem Size (# unknowns)	Dual AMD 7763 (128 cores @ 2.45 GHz) + A100 GPU				
	CPU Direct	CPU IFGF	Speedup	GPU IFGF	Speedup
5,895,600	4586 sec	394 sec	**11.6x**	13.7 sec	**335x**

Multi-Level IFGF

- How can we go from $O\left(N^{\frac{3}{2}}\right)$ to $O(NlogN)$?

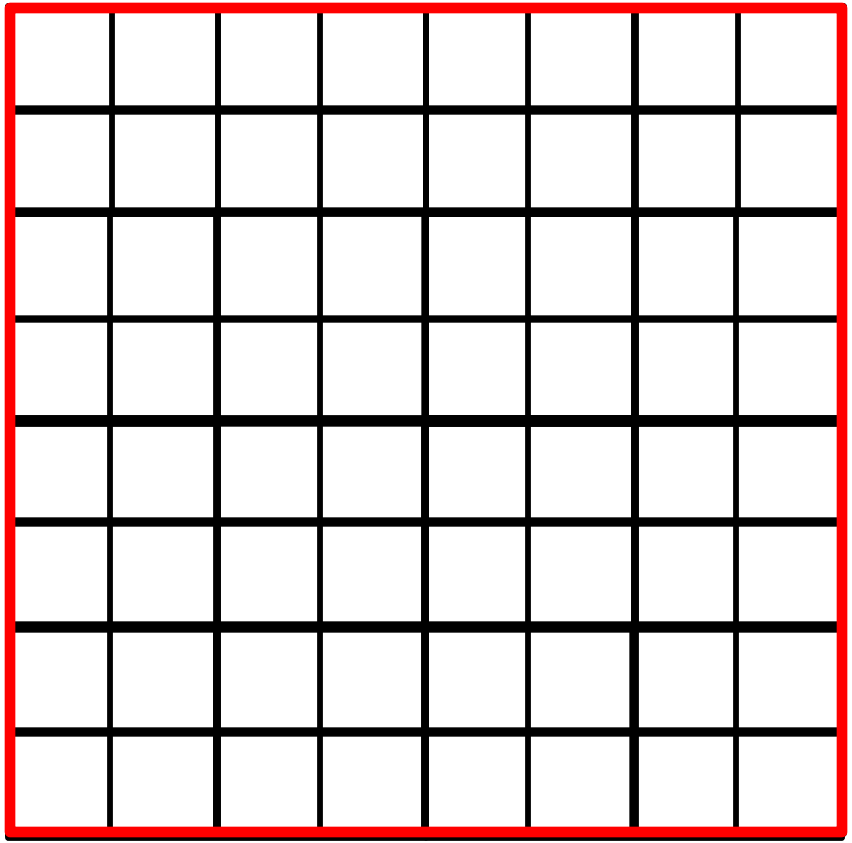

Multi-Level IFGF

- How can we go from $O\left(N^{\frac{3}{2}}\right)$ to $O(NlogN)$?
- Build an octree and use nested interpolation.

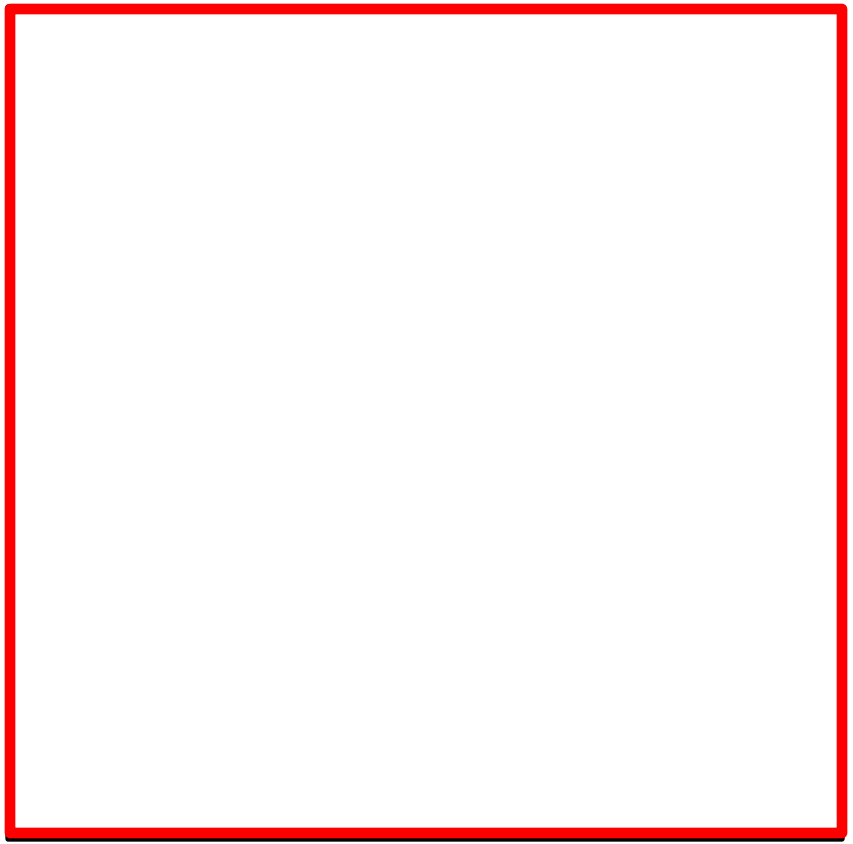

Level: d=1

Multi-Level IFGF

- How can we go from $O\left(N^{\frac{3}{2}}\right)$ to $O(NlogN)$?
- Build an octree and use nested interpolation.

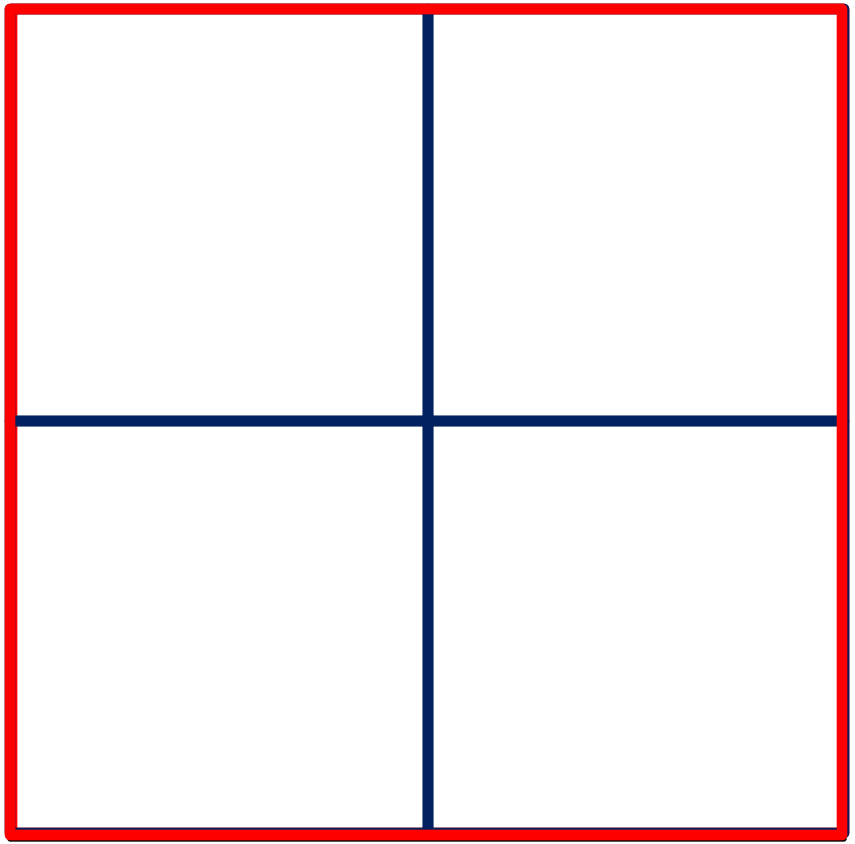

Level: d=2

Multi-Level IFGF

- How can we go from $O\left(N^{\frac{3}{2}}\right)$ to $O(NlogN)$?
- Build an octree and use nested interpolation.

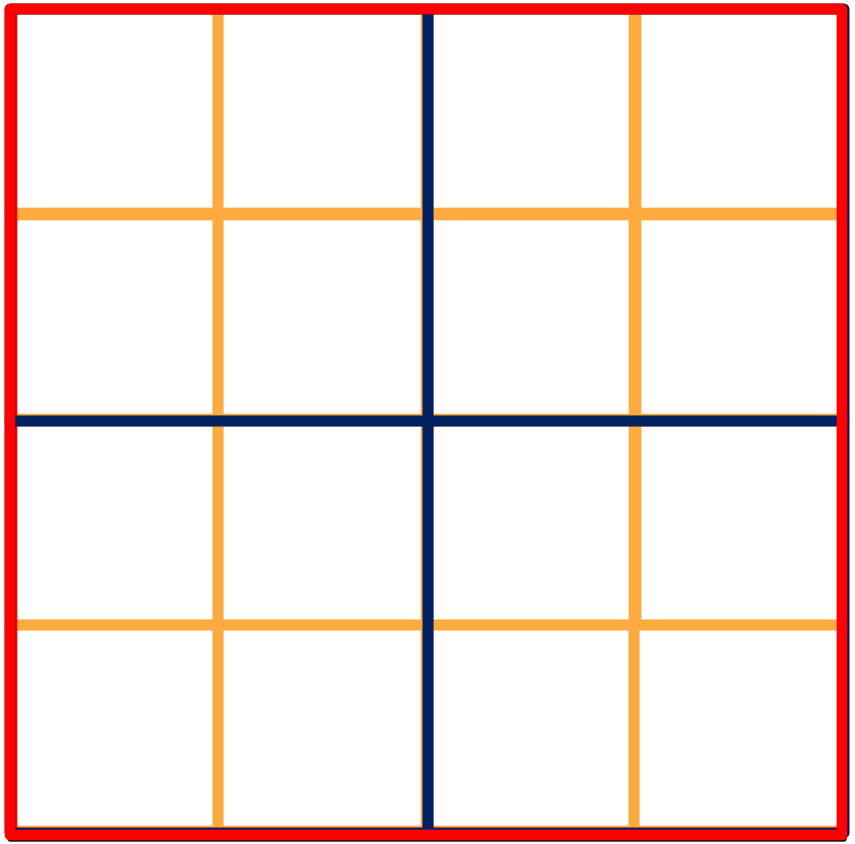

Level: d=3

Multi-Level IFGF

- How can we go from $O\left(N^{\frac{3}{2}}\right)$ to $O(NlogN)$?
- Build an octree and use nested interpolation.

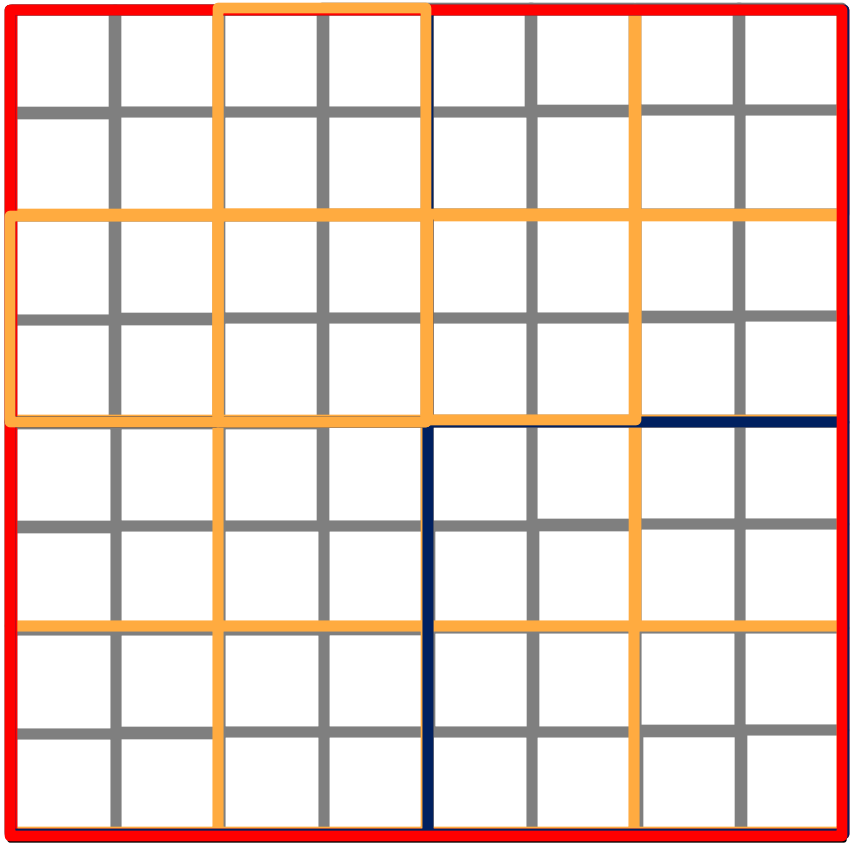

Level: d=4

Multi-Level IFGF

- How can we go from $O\left(N^{\frac{3}{2}}\right)$ to $O(NlogN)$?
- Build an octree and use nested interpolation.
- Start from lowest level (in this example, d=4)

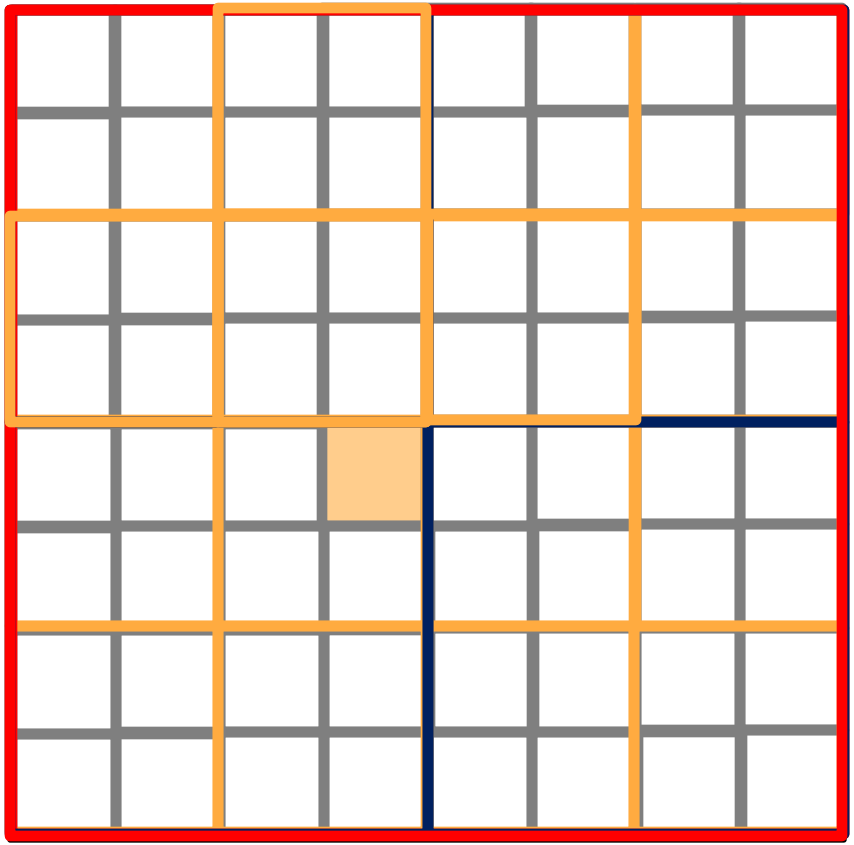

Level: d=4

Multi-Level IFGF

- How can we go from $O\left(N^{\frac{3}{2}}\right)$ to $O(NlogN)$?
- Build an octree and use nested interpolation.
- Start from lowest level (in this example, d=4) and use direct computation for all target points in neighboring boxes.

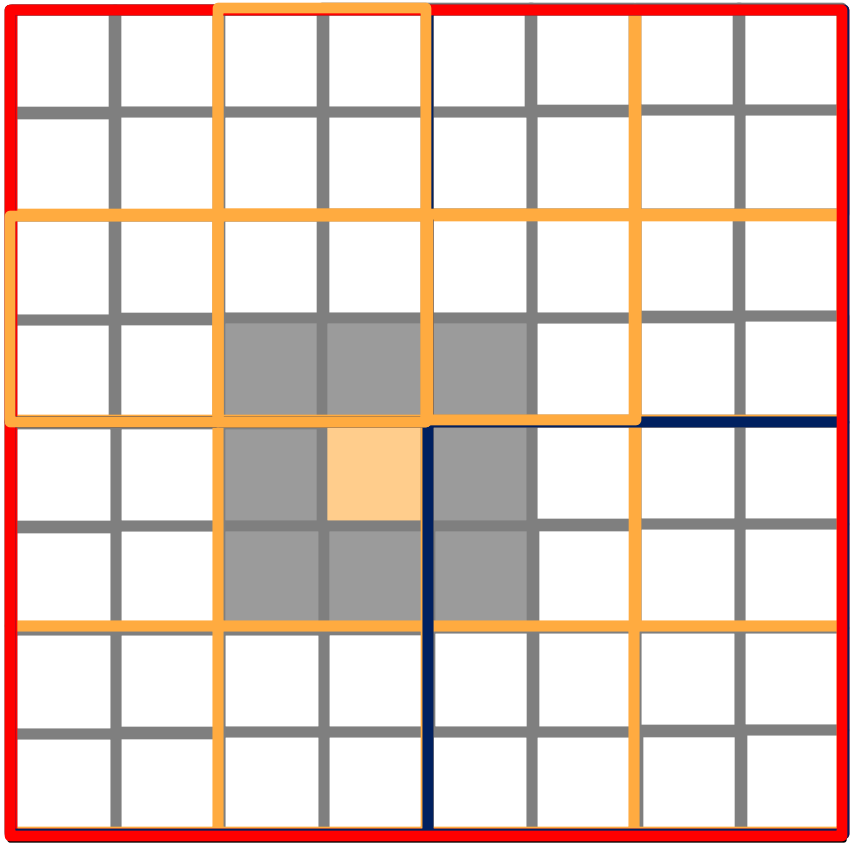

Level: d=4

Multi-Level IFGF

- Next use direct computation to compute cone interpolants at level d=4.

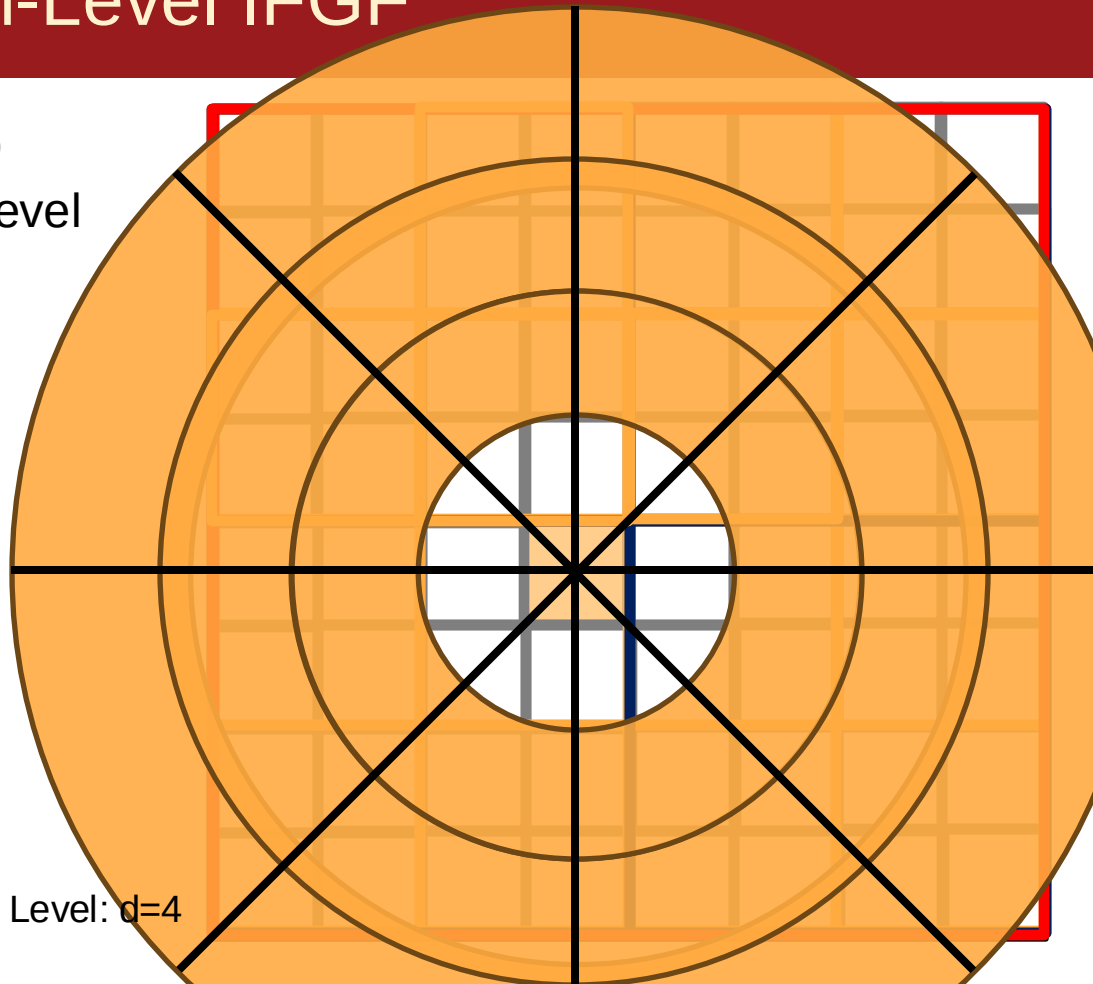

Multi-Level IFGF

- Next use direct computation to compute cone interpolants at level d=4.
- Use these cone interpolants to compute the values of target points in ”cousin” boxes: A ”cousin” box is box on the same level that is NOT a neighbor but is a child of a neighbor of the parent of the current box.
- Do **NOT** compute any more target points at this level for further away boxes– higher levels can be used for this.

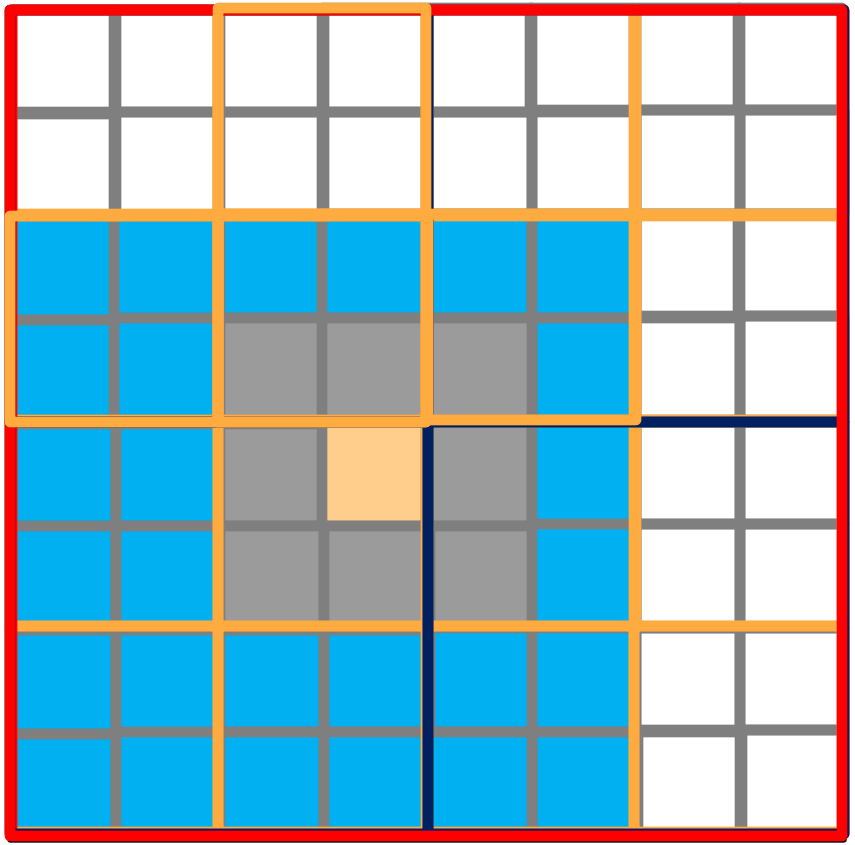

Level: d=4

Multi-Level IFGF

- Instead, use cone interpolants at level d to compute points needed to compute the cone interpolants for the next level up d-1 (in this case d=3).
- 8x cones one level higher, but 8x fewer boxes, so approx. constant O(N) operations per level
- ~$\log_2$ N levels due to octree splitting
- O(N log N) overall complexity after traversing through all levels

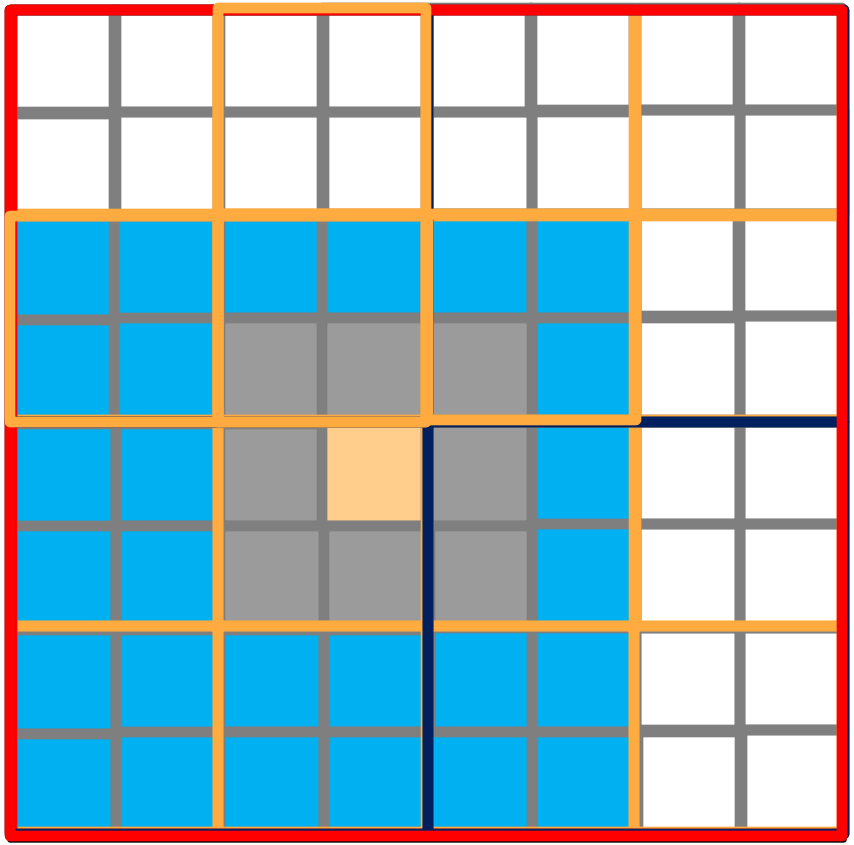

Level: d=4

Maxwell's Equations: PEC and Dielectric Case

- Consider the Magnetic Field Integral Equation (MFIE) for PECs:
- $\frac{\boldsymbol{J}}{2} + \mathcal{K}[\boldsymbol{J}] = \boldsymbol{n} \times \boldsymbol{H}^{inc}$ with $\mathcal{K}[\mathbf{a}](\mathrm{r}) = -\mathbf{n}(\boldsymbol{r}) \times \nabla \times \int_\Gamma G(\boldsymbol{r}, \boldsymbol{r}')\boldsymbol{a}(\boldsymbol{r}')d\sigma(\boldsymbol{r}')$
- $\mathcal{K}$ can be rewritten in terms of the single layer as:
- $$\mathcal{K}[\boldsymbol{a}](\boldsymbol{r}) = \frac{\partial}{\partial \boldsymbol{n}}\mathcal{S}[\boldsymbol{a}](\boldsymbol{r}) - \left(\boldsymbol{e}^1(\boldsymbol{r})\left[\boldsymbol{n}(\boldsymbol{r}) \cdot \frac{\partial}{\partial u}\right] + \boldsymbol{e}^2(\boldsymbol{r})\left[\boldsymbol{n}(\boldsymbol{r}) \cdot \frac{\partial}{\partial v}\right]\right)\mathcal{S}[\boldsymbol{a}](\boldsymbol{r})$$
- Similarly, N-Muller formulation for dielectrics can also be broken down into evaluations of the single layer and its normal derivative.
- Single layer $\mathcal{S}[\boldsymbol{a}](\boldsymbol{r}) = \int_\Gamma G(\boldsymbol{r}, \boldsymbol{r}')a(\boldsymbol{r}')d\sigma(\boldsymbol{r}')$ straightforward to accelerate with IFGF: Create an interpolant for each Cartesian component of the density.

- What about the normal derivative?

Maxwell's Equations: PEC and Dielectric Case

- IFGF cones comprise 3D Chebyshev polynomial approximations of the single layer operator within their spatial support: $g_s(u,v,w) = \sum_i \sum_j \sum_k \alpha_{ijk} T_i(u) T_j(v) T_k(w)$
- $\mathcal{S} = (\text{centered factor}) * g_s = \mathrm{G}(\mathbf{x}, \boldsymbol{y_c}) * g_s$

- $\frac{\partial}{\partial \boldsymbol{n}} \mathcal{S} = \lim_{h \to 0} \frac{\mathcal{S}(\boldsymbol{x}+\hat{\boldsymbol{n}}h) - \mathcal{S}(\boldsymbol{x})}{h} \approx \frac{\mathcal{S}(\boldsymbol{x}+\hat{\boldsymbol{n}}h) - \mathcal{S}(\boldsymbol{x})}{h}$ for h>0.

- Easily computed with one additional IFGF single layer evaluation a distance h away from the target point $\mathbf{x}$ in the normal direction.

- Faster than analytically computing derivatives of the IFGF Chebyshev expansions and no accuracy impact for small enough h.

Multi-Level IFGF: Dielectric Sphere

$$\epsilon_{ext} = 1.0, \epsilon_{int} = 2.25$$

Problem Size (# unknowns)		Dual AMD 7763 (128 cores @ 2.45 GHz)		
	$k_{interior}$	CPU Direct (sec)	CPU IFGF	Speedup
24,576	3π	0.064	0.076	**X**
98,304	6π	0.909	0.440	**2.1x**
393,216	12π	13.05	2.25	**5.8x**
1,572,864	24π	151.05	10.85	**13.9x**
6,291,456	48π	2463.5	50.14	**49.1x**

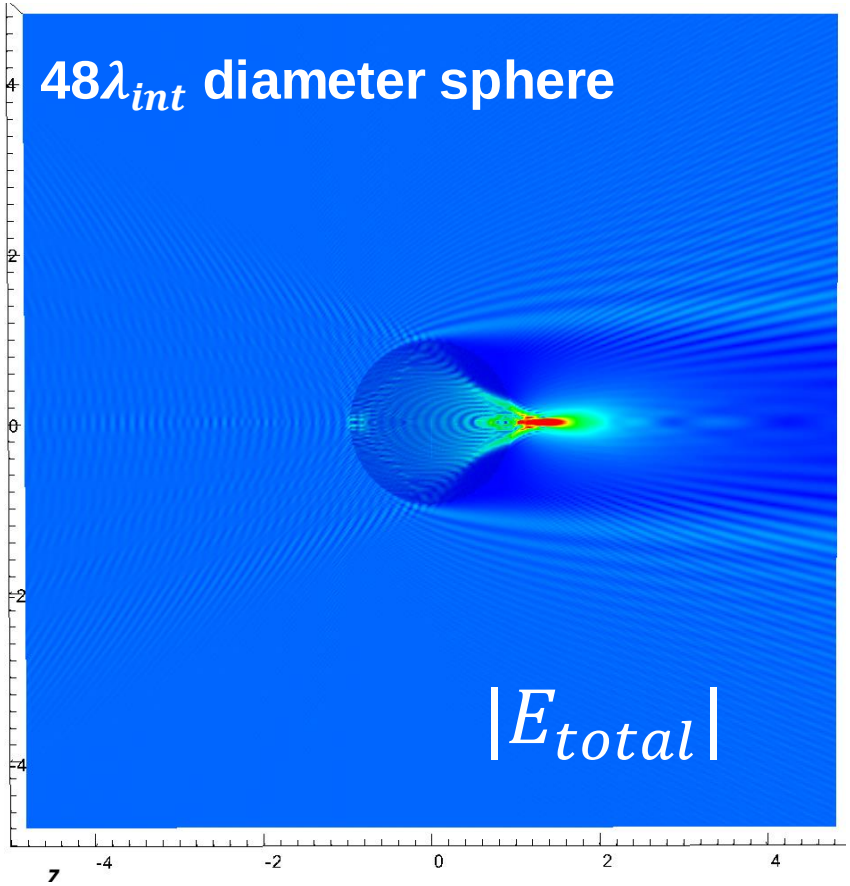

Multi-Level IFGF: Dielectric Sphere

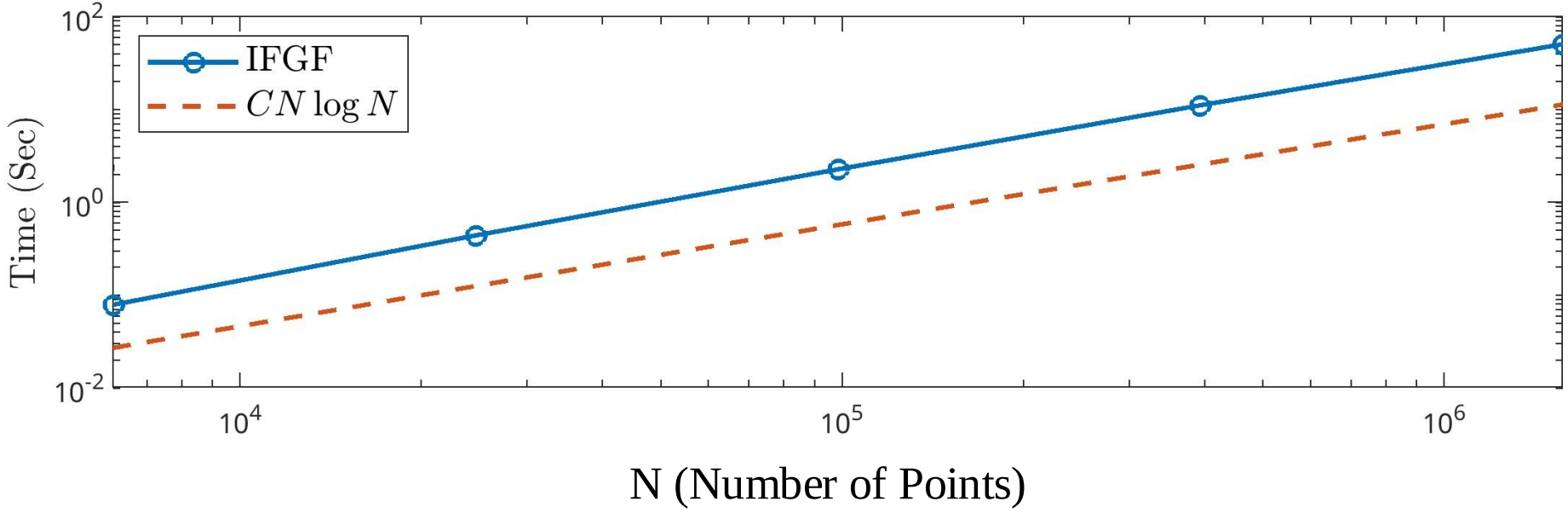

Additional Examples: Glider

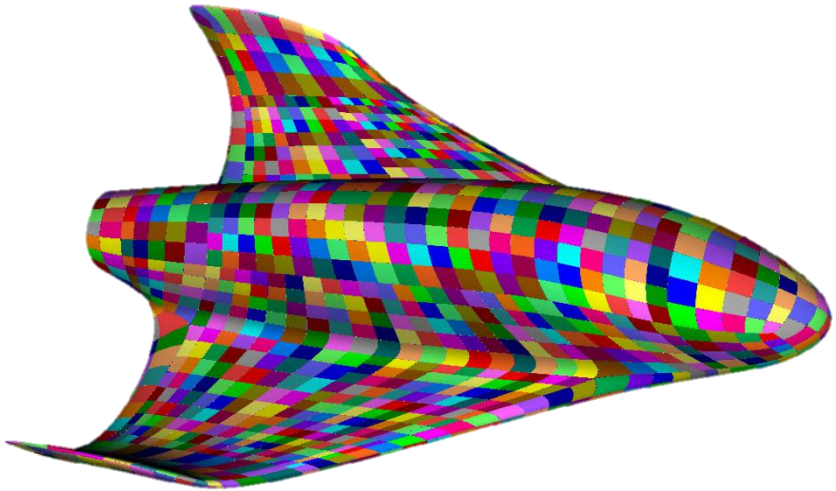

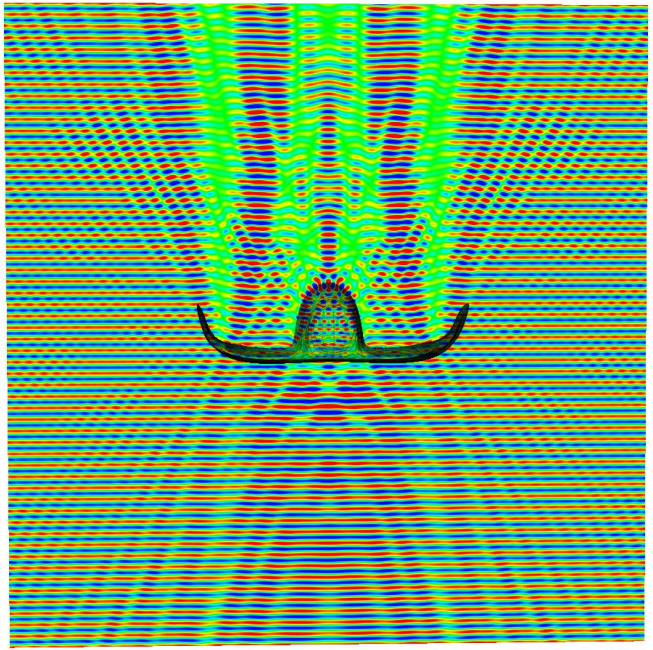

- 45-wavelength in longest dimension ($\epsilon_r^e = 1, \epsilon_r^i = 2.16;\ k_e = 25.1, k_i = 36.9$)
- N = 1,281,600 unknowns
- 9 sec for forward map using IFGF vs. 110 without acceleration **(12.2x speedup)**

Additional Examples: Hummingbird

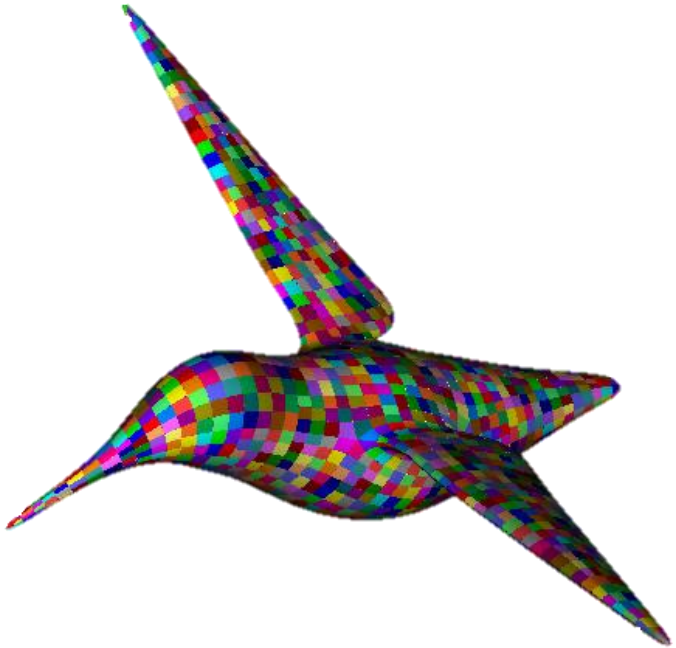

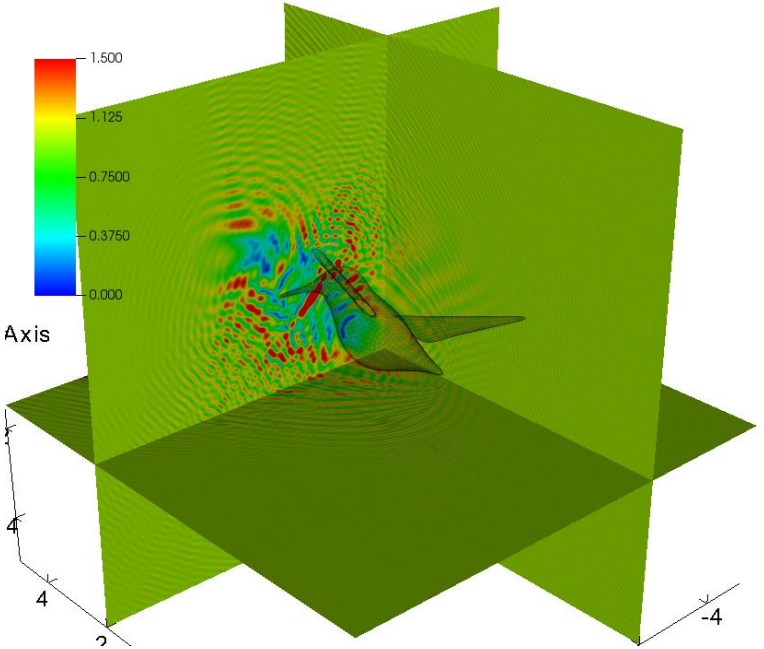

- 77-wavelength wingspan ($\epsilon_r^e = 1, \epsilon_r^i = 2.16;\ k_e = 50.3, k_i = 73.9$)
- N = 2,723,328 unknowns
- 27 sec for forward map using IFGF vs. 588 without acceleration **(22x speedup)**

Additional Examples: Nanophotonic Power Splitter

Re(Ex)

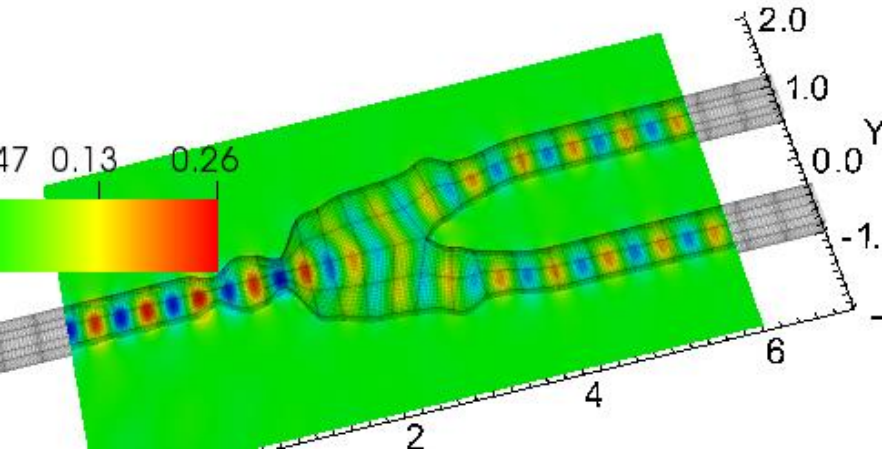

Abs(Ex)

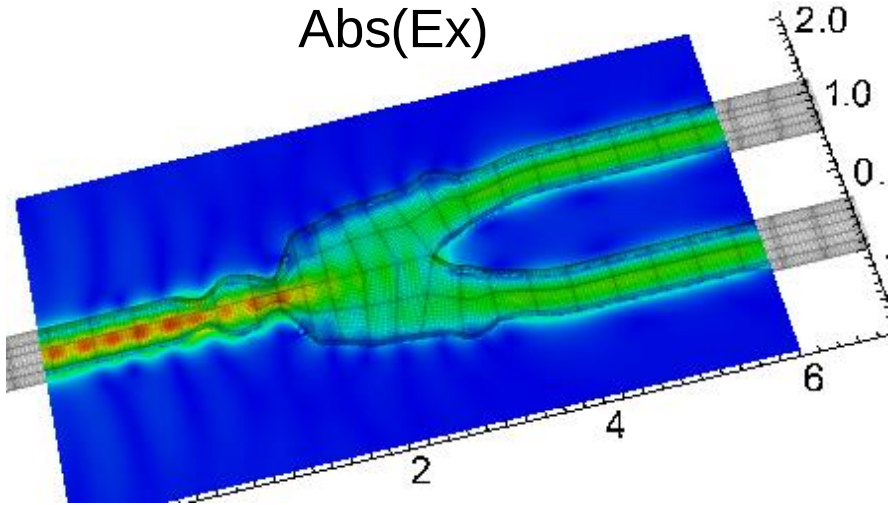

- 77-wavelength wingspan ($\epsilon_r^e = 2.08, \epsilon_r^i = 12.08;\ k_e = 5.85, k_i = 14.09$)
- N = 161,280 unknowns
- 0.5 sec for forward map using IFGF vs. 2.5 without acceleration **(5x speedup)**

Outline

1. Introduction
2. The Multi-Level Interpolated Green Function (IFGF) Method for 3D Maxwell
3. **Corner Regularized Combined Field Integral Equations (CR-CFIE) for Scattering from Objects with Geometric Singularities**
4. The Precomputed Numerical Green Function (PNGF) Method for Ultra-fast Inverse Design
   a) Introduction to PNGF
   b) Applications to metallic RF devices
   c) Applications to dielectric nanophotonic devices
5. Conclusions

Introduction: Corner Regularized Integral Equations

- Fields at edges/corners for PECs tend to infinity or 0 algebraically.
- Near the corner, the behavior is well modeled by quasistatic fields and the exponent is dependent on the angle[1]
- Polynomial basis functions are poor approximators of these singular fields
- Convergence of high-order methods significantly suffers for non-smooth geometries with sharp edges or corners.

Sideris, C., Aslanyan, D., and Bruno, O. "High-order-accurate Solution of Scattering Integral Equations with Unbounded Solutions at Corners". In preparation.

TM Mode (Hz, Ex, Ey)

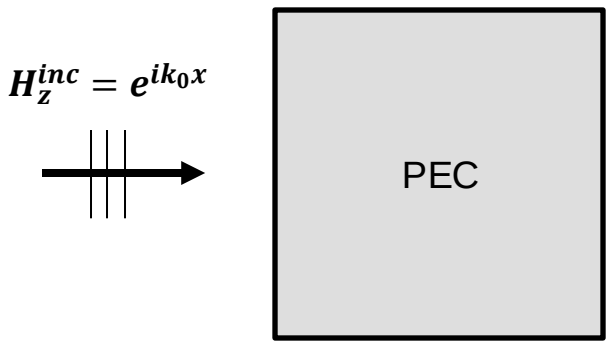

[1] Zargaryan SS, Mazya VG (1984) The asymptotic form of the solutions of integral equations of potential theory in theneighborhood of the corner points of a contour. Prikl Mat Mekh 48:169–174

CBIE Convergence: PEC Circle vs. Square Geometry

- $u^{scat}(\boldsymbol{r}) = \sum_p \int_{\Gamma p} \int_{-1}^{1} \frac{dG(\boldsymbol{r},\boldsymbol{r}'(\theta))}{dn(\boldsymbol{r})} \phi^p(\boldsymbol{r}'(\theta))\tau(\theta)d\theta = \sum_p \mathcal{K}[\phi^p]$ with $\tau = \frac{d\ell}{d\theta}$ being the line element and the density on each patch: $\phi^p(\theta) = \sum_n \alpha_n^p T_n(\theta)$
- Test using point-matching on same grid as unknowns: $\left[\frac{I}{2} - K\right]\phi = \frac{dH_z^{inc}}{dn(r)}$

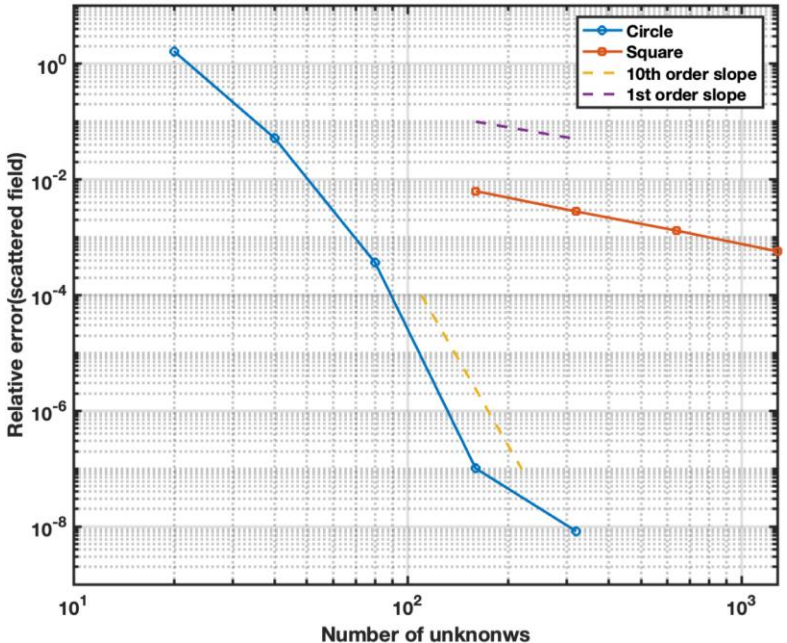

- Zero centered circle (D=2) and square (edge length = 2)
- $\lambda_0 = 0.628$
- Incident field: $H_z^{inc} = e^{ik_0 x}$
- N=10 points patch
- Target point for comparison: (1.5, 1.5).
- Circle achieves expected 10th order convergence slope.
- Square suffers from poor 1st order convergence.

Last Year: PEC Objects with Sharp Edges: MFIE

- Consider TM case with incident plane wave excitation: $H_z^{inc} = e^{ik_0 x}$
- Representation theorem: $H_z^{scat} = \int_\Gamma G(r,r')\phi(r')d\ell(r')$
- MFIE satisfying Neumann boundary conditions: $\frac{dH_z^{scat}}{dn} + \frac{dH_z^{inc}}{dn} = 0$
- Corresponding integral equation:
- $$-\frac{1}{2}\phi(r) + \frac{d}{dn(r)}\int_\Gamma G(r,r')\phi(r')d\ell(r') = -\frac{dH_z^{inc}}{dn(r)}$$

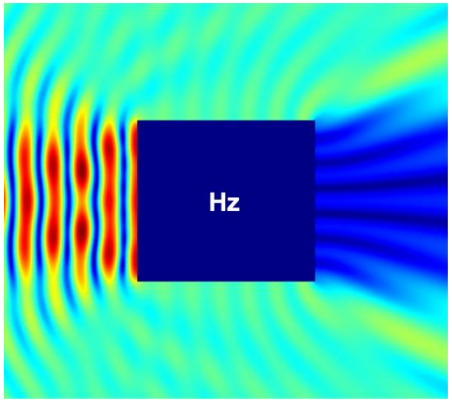

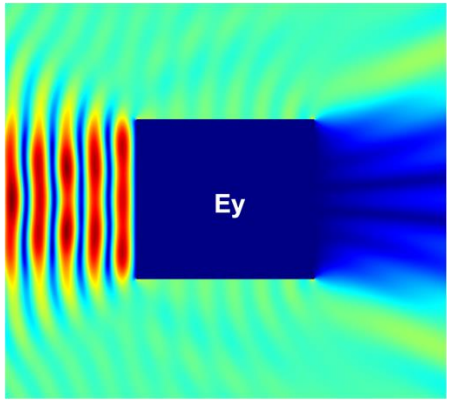

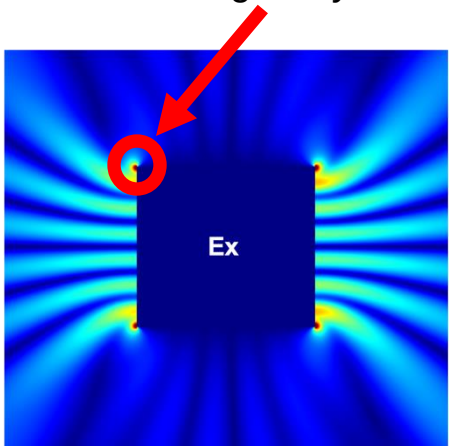

Last Year: Modified CBIE Approach for MFIE

- BIEs with Neumann boundary conditions have operators similar to the 3D case (e.g., hypersingular operator, target point normal derivatives, etc.)
- Introduce 1:1 change of variables (CoV) for patches with corners, e.g.: $s(\theta) = \theta^p$.
- Integral for source patch q' with CoV with target point on patch q becomes:
- $\int_0^1 \frac{dG_k\left(\tilde{\boldsymbol{r}}_q(\theta), \tilde{\boldsymbol{r}}_{q'}(\theta')\right)}{d\boldsymbol{n}\left(\tilde{\boldsymbol{r}}_q(\theta)\right)} \phi_{q'}(\theta')\tilde{L}_{q'}(\theta')d\theta'$ where $\tilde{\boldsymbol{r}}_q(\theta) = \boldsymbol{r}_{\boldsymbol{q}}(s_q(\theta))$ and $\tilde{L}_{q'}(\theta') = \frac{d\ell}{ds_q}\frac{ds_q(\theta')}{d\theta'} = L_{q'}(s(\theta'))\frac{ds_q(\theta')}{d\theta'}$ is the new line element.

- **NOTE:** $p-1$ derivatives of $s(\theta)$ are 0 at $\theta = 0$, may cancel the singularity in ϕ
- MFIE with CoV for system with M patches becomes:

$$-\frac{1}{2}\phi_q(\boldsymbol{\theta}) + \sum_{q'=1}^{M}\int_0^1 \frac{dG\left(\tilde{\boldsymbol{r}}_q(\theta), \tilde{\boldsymbol{r}}_{q'}(\theta')\right)}{d\boldsymbol{n}\left(\tilde{\boldsymbol{r}}_q(\theta)\right)} \phi_{q'}(\theta')\tilde{L}_{q'}(\theta')d\theta' = -\frac{dH_z^{inc}}{d\boldsymbol{n}\left(\tilde{\boldsymbol{r}}_q(\theta)\right)}$$

Last Year: Modified Approach for MFIE (Cont.)

- Multiply integral equation through by target point line element, $\tilde{L}_q(\theta)$:
- $-\frac{1}{2}\tilde{L}_q(\theta)\phi_q(\theta) + \tilde{L}_q(\theta)\sum_{q'=1}^{M}\int_0^1 \frac{dG\left(\tilde{\boldsymbol{r}}_q(\theta),\tilde{\boldsymbol{r}}_{q'}(\theta')\right)}{d\boldsymbol{n}\left(\tilde{\boldsymbol{r}}_q(\theta)\right)}\phi_{q'}(\theta')\tilde{L}_{q'}(\theta')d\theta' = -\frac{dH_z^{inc}}{d\boldsymbol{n}\left(\tilde{\boldsymbol{r}}_q(\theta)\right)}\tilde{L}_q(\theta)$
- Define new unknown: $\psi_q(\theta) = \phi_q(\theta)\tilde{L}_q(\theta)$ and solve for:

$$-\frac{1}{2}\psi_q(\theta) + \tilde{L}_q(\theta)\sum_{q'=1}^{M}\int_0^1 \frac{dG\left(\tilde{\boldsymbol{r}}_q(\theta),\tilde{\boldsymbol{r}}_{q'}(\theta')\right)}{d\boldsymbol{n}\left(\tilde{\boldsymbol{r}}_q(\theta)\right)}\psi_{q'}(\theta')d\theta' = -\frac{dH_z^{inc}}{d\boldsymbol{n}\left(\tilde{\boldsymbol{r}}_q(\theta)\right)}\tilde{L}_q(\theta)$$

- $\psi_q(\theta)$ is easier to approximate using polynomials than the original ϕ density since the $\tilde{L}_q(\theta)$ line element due to the CoV makes it (and p-1 of its derivatives) go to 0 at $\theta = 0$ where the field singularity is located.
- Multiplication by line element forces the incident field(RHS) to go to zero at the corners ⇒ density also tends to 0 at the corner due to identity.

PEC Objects with Sharp Edges: CFIE

- The TM MFIE equation has resonances and is not uniquely solvable
- Consider the representation theorem[7,8,9]: $H_z^{scat}(\boldsymbol{r}) = -i\int_\Gamma G_k(\boldsymbol{r},\boldsymbol{r}')\phi(\boldsymbol{r}')d\ell(\boldsymbol{r}') + \int_\Gamma \frac{dG_k(\boldsymbol{r},\boldsymbol{r}')}{d\boldsymbol{n}(r')}\phi(\boldsymbol{r}')d\ell(\boldsymbol{r}')$
- TM CFIE satisfying Neumann boundary conditions: $\frac{dH_z^{scat}}{d\boldsymbol{n}} + \frac{dH_z^{inc}}{d\boldsymbol{n}} = 0$
- Corresponding combined field integral equation:
- $\underbrace{\frac{i\eta}{2}\phi(\mathbf{r}) - i\eta T_1[\phi](\boldsymbol{r})}_{\text{MFIE}} + \underbrace{k^2 T_2[\phi](\boldsymbol{r}) + T_3[\phi](\boldsymbol{r})}_{\text{EFIE}} = -\frac{dH_z^{inc}}{dn(r)}$
- $T_1[\phi](\boldsymbol{r}) = \int_\Gamma \frac{dG_k(\boldsymbol{r},\boldsymbol{r}')}{d\boldsymbol{n}(\boldsymbol{r})}\phi(\boldsymbol{r}')d\ell(\boldsymbol{r}')$
- $T_2[\phi](\boldsymbol{r}) = \int_\Gamma G_k(\boldsymbol{r},\boldsymbol{r}')(\boldsymbol{n}(\boldsymbol{r})\cdot\boldsymbol{n}'(\boldsymbol{r}'))\,\phi(\boldsymbol{r}')d\ell(\boldsymbol{r}')$
- $T_3[\phi](\boldsymbol{r}) = \partial_{\tau(\boldsymbol{r})}\int_\Gamma G_k(\boldsymbol{r},\boldsymbol{r}')\partial_{\tau(\boldsymbol{r}')}\phi(\boldsymbol{r}')d\ell(\boldsymbol{r}')$

CFIE system is badly conditioned due to the hypersingular kernel of EFIE operator

[7] Burton, A., Miller J., The application of integral equation methods to the numerical solution of some exterior boundary-value problems, Proc. Royal Soc. London 323 (1971), 201-210

[8] Burton, A., Numerical solution of acoustic radiation problems, NPL Contract Rept. OC5/S35 National Physical Laboratory, Teddington, Middlesex, (1976).

[9] Brackhage H, Werner P. Uber das Dirichletsche aussenraumproblem fur die Helmholtsche schwingungsgleichung. Archiv der Mathematik 1965; 16:325–329.

Modified CBIE Approach: CR-CFIE

- We can add a regularization operator to the EFIE[11]:

$$R[\phi] = \int_{\Gamma} G_{ik}(\boldsymbol{r}, \boldsymbol{r}'')\, \phi(\boldsymbol{r}'') d\ell(\boldsymbol{r}'')$$

- Then the EFIE part will take the form:

$$k^2 \int_{\Gamma} G_k(\boldsymbol{r}, \boldsymbol{r}')\big(\boldsymbol{n}(\boldsymbol{r}) \cdot \boldsymbol{n}(\boldsymbol{r}')\ \big) R[\phi] d\ell(\boldsymbol{r}') + \frac{d}{d\tau(\boldsymbol{r})} \int_{\Gamma} G_k(\boldsymbol{r}, \boldsymbol{r}') \frac{d}{d\boldsymbol{r}'} R[\phi]\, d\ell(\boldsymbol{r}') = -\frac{dH_z^{inc}}{d\boldsymbol{n}(\boldsymbol{r})}$$

- Parameterize and consider the 1:1 change of variables (CoV) for patches with corners like before, the discretized regularization operator takes the form:

$$R[\phi](\tilde{\boldsymbol{r}}_{q'}(\theta')) = \sum_{q'=1}^{M} \int_0^1 G_{ik}\left(\tilde{\boldsymbol{r}}_{q'}(\theta'), \tilde{\boldsymbol{r}}_{q''}(\theta'')\right) \phi_{q''}\left(\tilde{\boldsymbol{r}}_{q''}(\theta'')\right) \tilde{L}_{q''}(\theta'')\, d\theta''$$

- NOTE: Regularization introduces the line element $\tilde{L}_{q''}(\theta'')$ next to the density which can be absorbed into the unknowns

[11] Bruno, O., Elling, T. and Turc, C. (2012), Regularized integral equations and fast high-order solvers for sound-hard acoustic scattering problems. Int. J. Numer. Meth. Engng, 91: 1045-1072.

The Corner Regularized CFIE: CR-CFIE

- Multiplying through by the line element $\tilde{L}_q(\theta)$ as was done for the MFIE and replacing the unknown with ψ, the final CR-CFIE is obtained:

$$\frac{i\eta}{2}\psi_q(\theta) - i\eta\tilde{L}_q(\theta)\sum_{q'=1}^{M}\int_0^1 \frac{dG_k\left(\tilde{\boldsymbol{r}}_q(\theta),\tilde{\boldsymbol{r}}_{q'}(\theta')\right)}{d\boldsymbol{n}\left(\tilde{\boldsymbol{r}}_q(\theta)\right)}\psi_{q'}(\theta')d\theta'$$

CR-MFIE

$$+ k^2\tilde{L}_q(\theta)\sum_{q'=1}^{M}\int_0^1 G_k\left(\tilde{\boldsymbol{r}}_q(\theta),\tilde{\boldsymbol{r}}_{q'}(\theta')\right)\left(\boldsymbol{n}\left(\tilde{\boldsymbol{r}}_q(\theta)\right)\cdot\boldsymbol{n}\left(\tilde{\boldsymbol{r}}_{q'}(\theta')\right)\right)\tilde{L}_{q'}(\theta')R[\psi]d\theta'$$

$$+ \frac{\partial}{\partial\theta}\sum_{q'=1}^{M}\int_0^1 G_k\left(\tilde{\boldsymbol{r}}_q(\theta),\tilde{\boldsymbol{r}}_{q'}(\theta')\right)\frac{\partial}{\partial\theta'}R[\psi]d\theta' = -\frac{dH_z^{inc}}{d\boldsymbol{n}\left(\tilde{\boldsymbol{r}}_q(\theta)\right)}\tilde{L}_q(\theta)$$

CR-EFIE

Comparison: TM MFIE vs TM R-ICFIE on a Square

- The TM MFIE equation has resonances and is not uniquely solvable, however the CFIE does not have resonances and is uniquely solvable

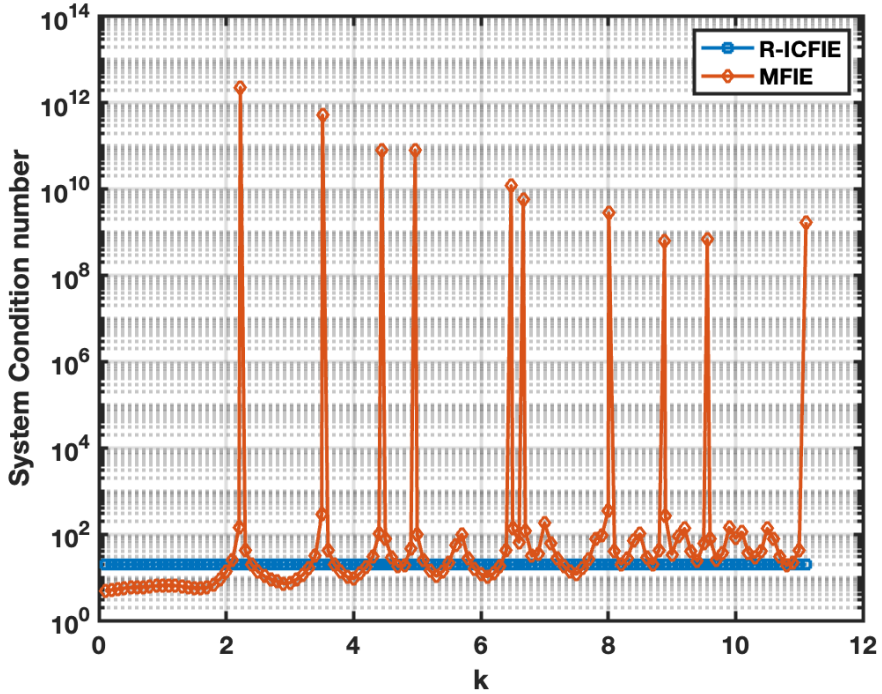

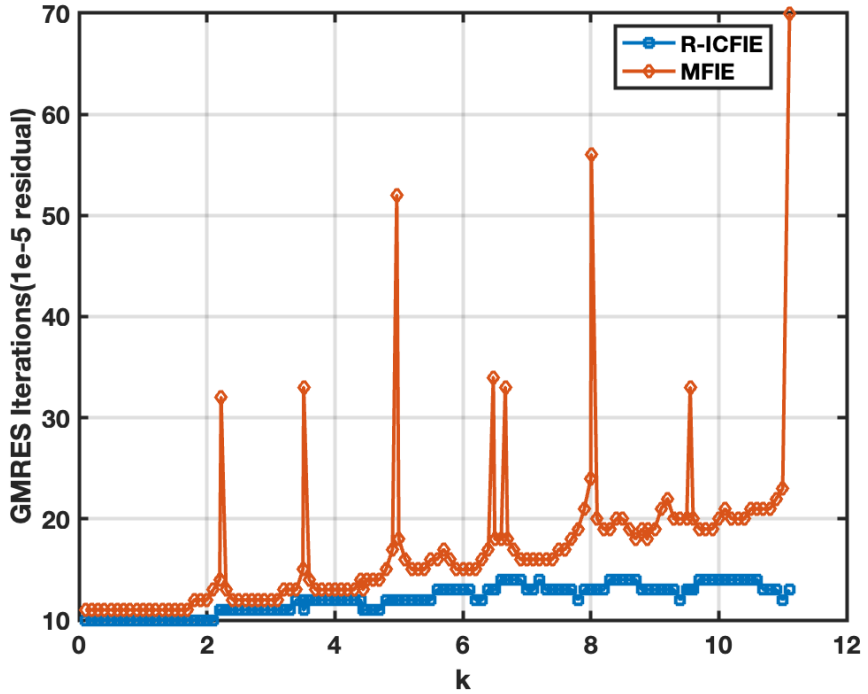

Numerical Results: Square

- Comparison of scattered field convergence for a point near the corner: $d = \mathbf{10^{-2}}$ (left) and $d = \mathbf{10^{-8}}$(right) ,$\mathrm{k}_0 = 10$ $(\lambda_0 = 0.63)$

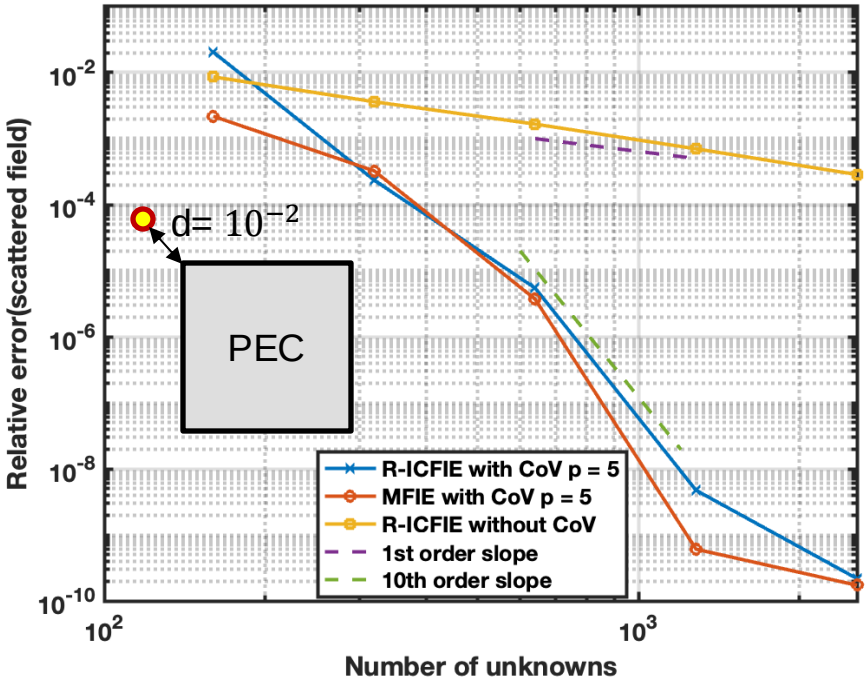

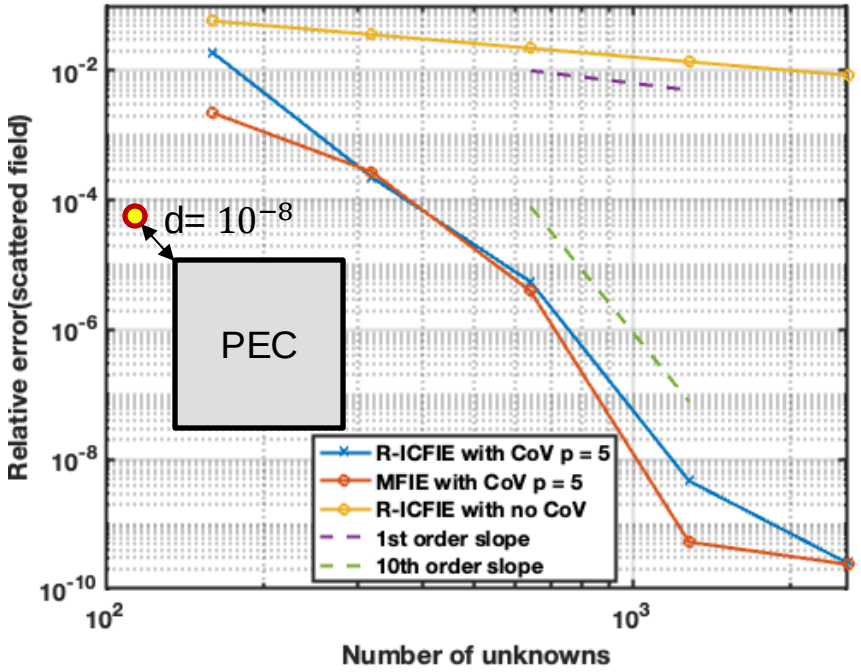

Numerical Results: Teardrop

- TM mode Total(Incident + Scattered) field distribution: Incident Plane wave excitation, PEC scatterer in the form of a Teardrop, $\mathrm{k}_0 = 10 \ (\lambda_0 = 0.63)$

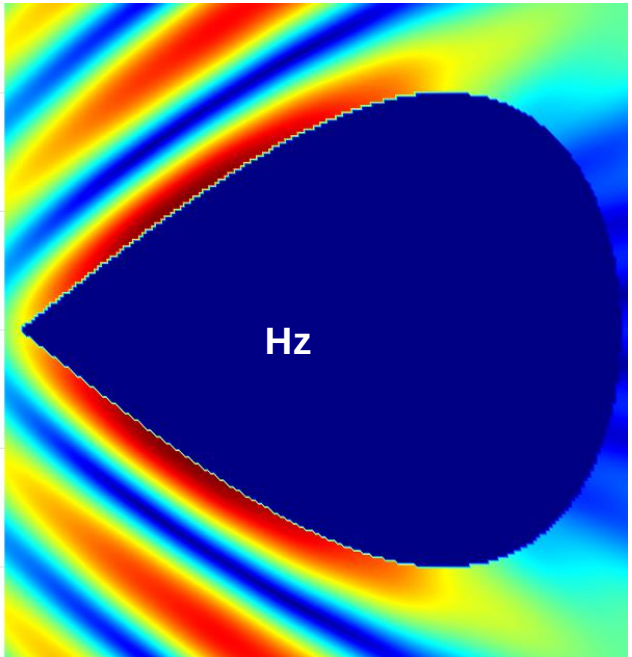

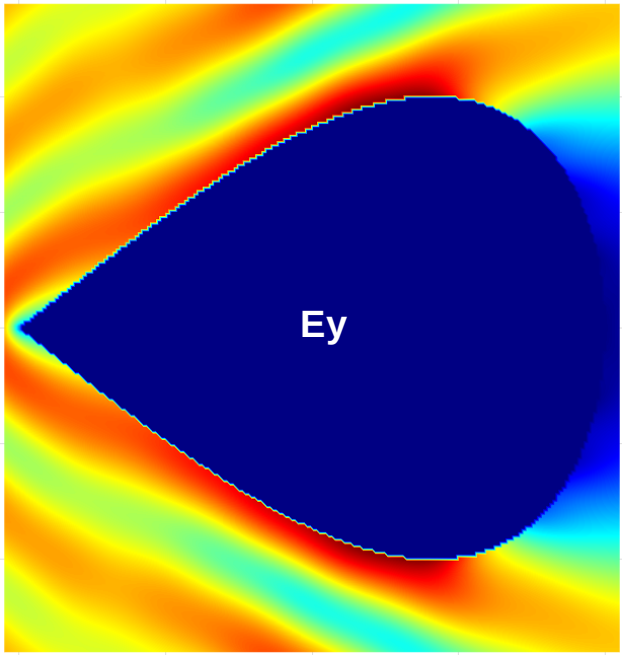

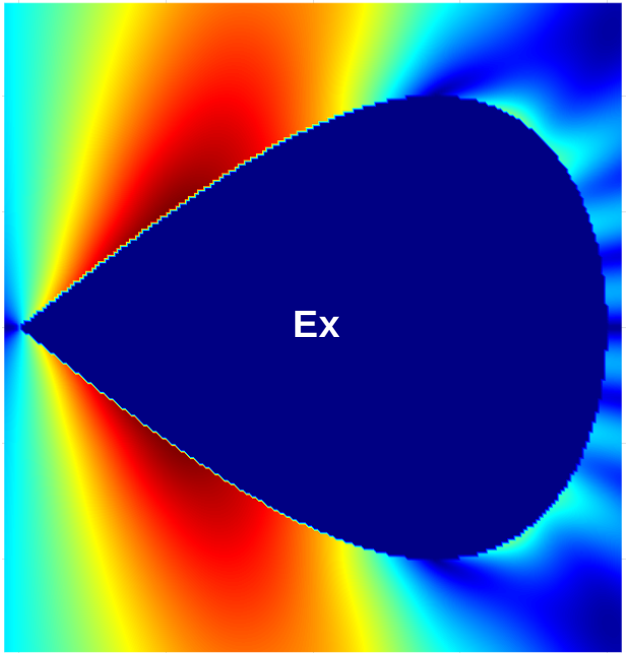

Numerical Results: Teardrop

- Comparison of scattered field convergence for a point near the corner: $d = \mathbf{0.5}$ (left) and $d = \mathbf{10^{-8}}$(right) ,$\mathrm{k}_0 = 10 \quad (\lambda_0 = 0.63)$

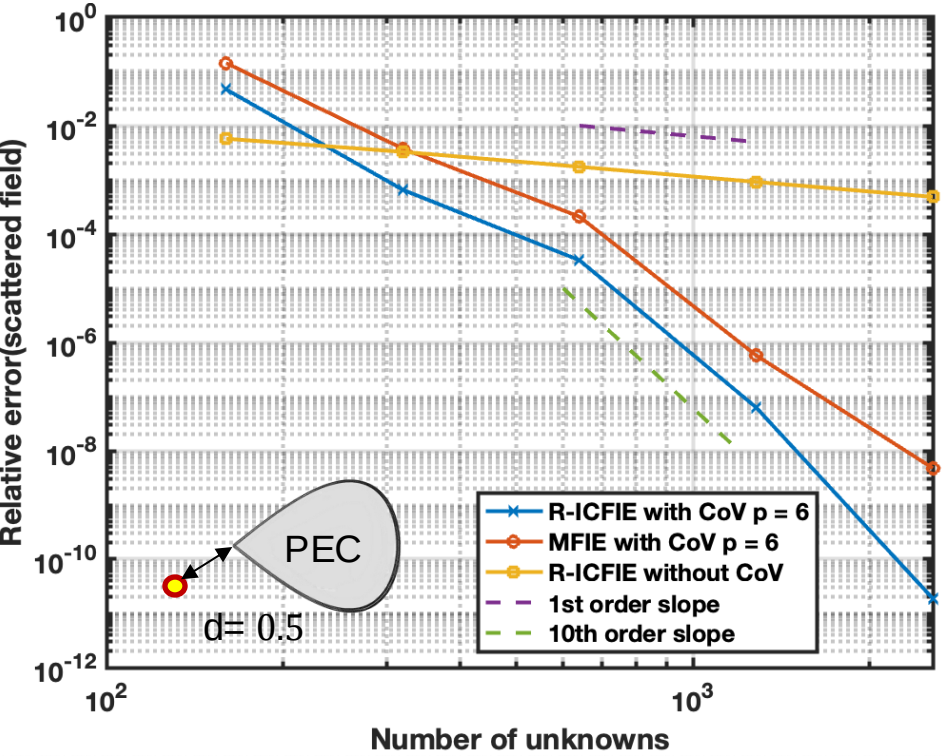

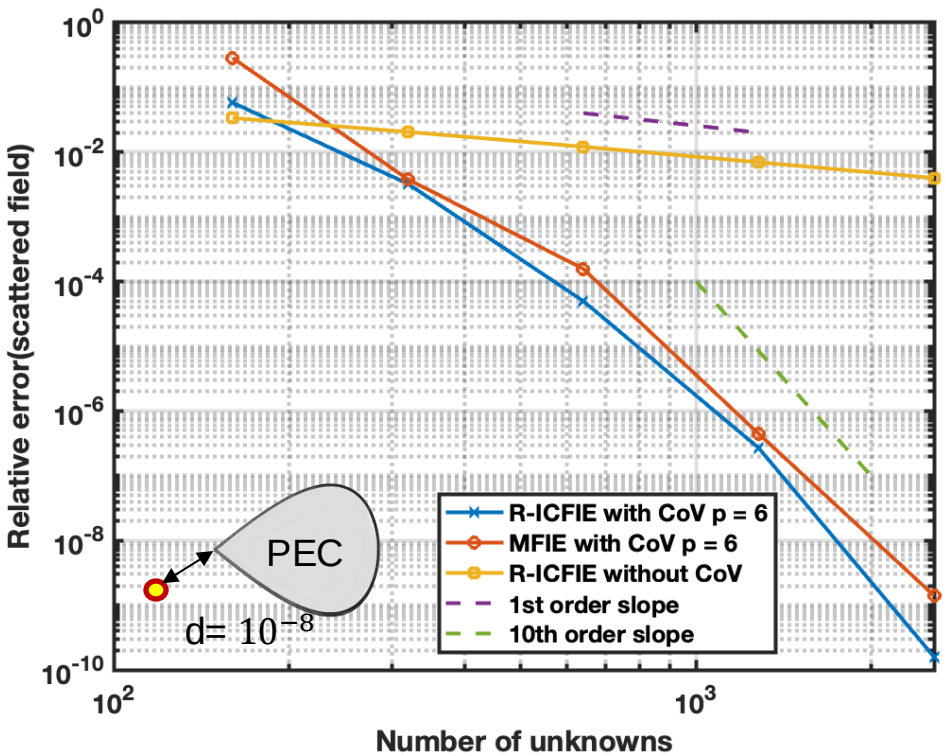

Outline

1. Introduction
2. The Multi-Level Interpolated Green Function (IFGF) Method for 3D Maxwell
3. Corner Regularized Combined Field Integral Equations (CR-CFIE) for Scattering from Objects with Geometric Singularities
4. **The Precomputed Numerical Green Function (PNGF) Method for Ultra-fast Inverse Design**
   a) Introduction to PNGF
   b) Applications to metallic RF devices
   c) Applications to dielectric nanophotonic devices
5. Conclusions

From Last Year: Ultra-fast Antenna Design

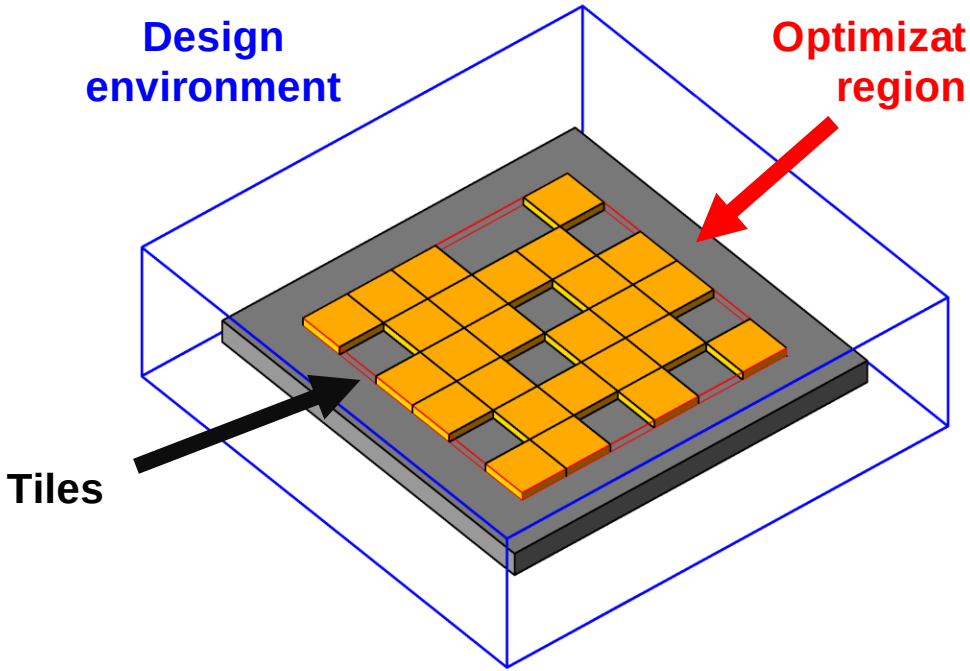

Zheng, Y. and **Sideris, C.** "Ultra-fast Simulation and Inverse Design of Metallic Antennas". IEEE International Microwave Symposium (2023).

Zheng, Y., Elsawaf, M., Hung, J., Lin, H.-C., Hsu, C.W., **Sideris, C.** ""Ultra-fast Inverse Design of Radio-Frequency Electromagnetic Devices". In preparation.

- Pixelated electromagnetic structures made up of a grid of tiles, each of which is either filled with metal or left empty, in a predefined optimization region

Current Equivalence Principle

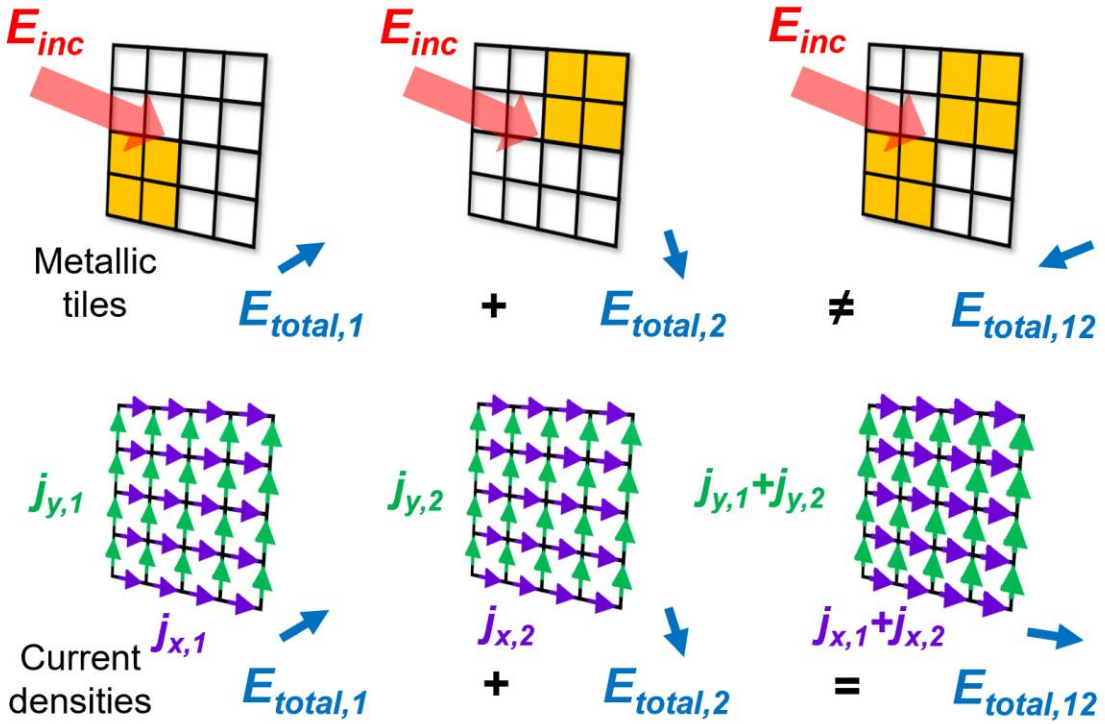

- Fields due to scattering from metals do not satisfy additivity
- However, tiles can be replaced with equivalent current densities

Leveraging Current Equivalence

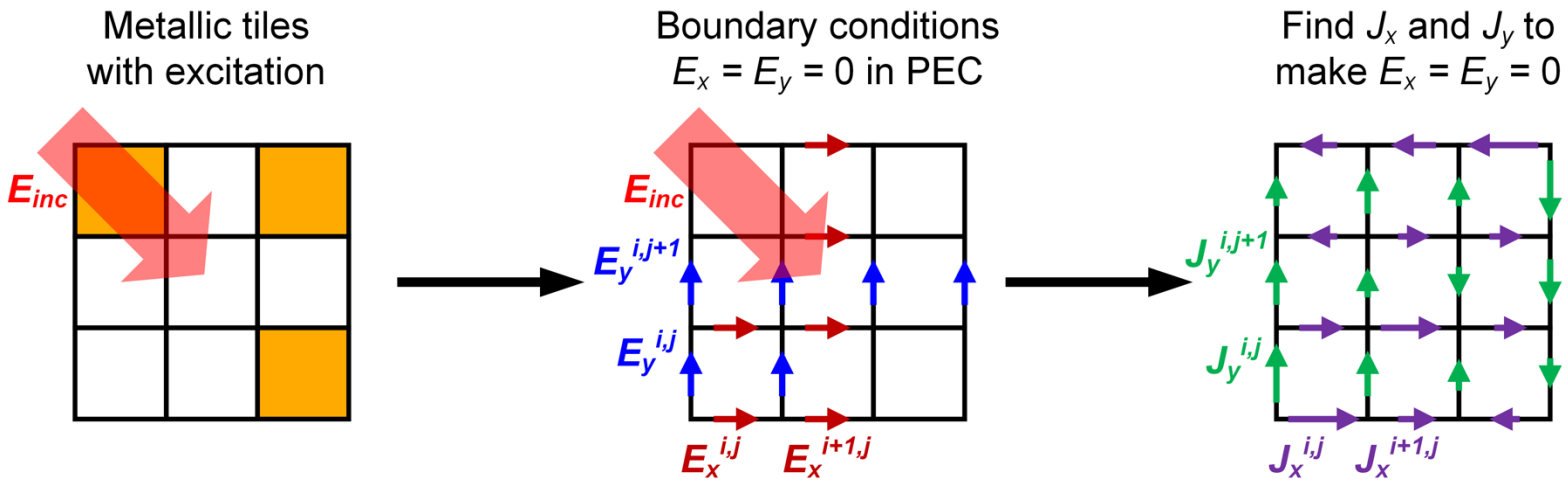

- Choose values for surface j's to enforce $E_{tan} = 0$ over desired PEC region
- Find a **numerical Green function** (NGF) G: $J_{surf} \rightarrow E_{tan}$ that maps equivalent currents in the optimization region to corresponding electric fields in the same region

*Y. Zheng and **C. Sideris** "Ultra-fast Simulation and Inverse Design of Metallic Antennas". IEEE IMS 2023.

Numerical Green Function

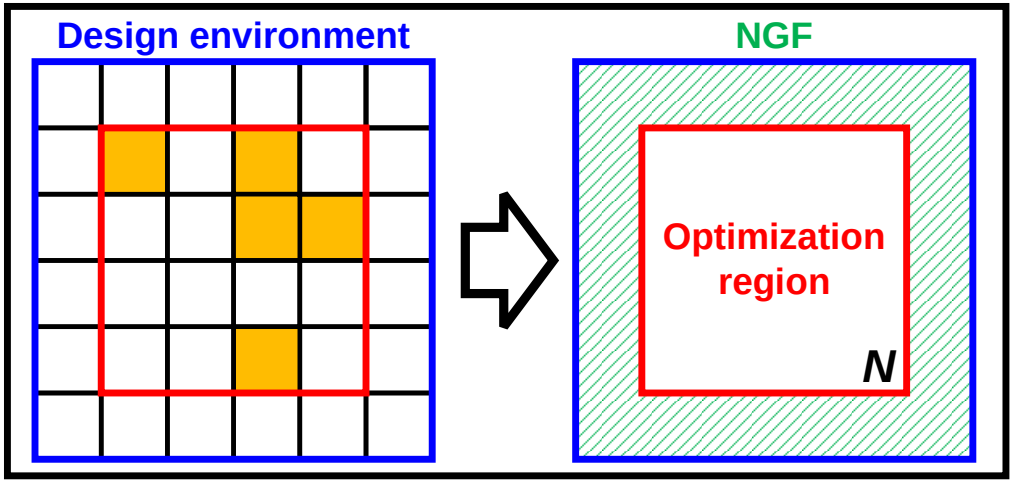

- NGF incorporates effect of the static environment outside the optimization region
- Allows candidate designs to be evaluated by solving a linear system over the optimization region only, as opposed to the entire design environment
- **Ultra-fast approach**: Timescale of **milliseconds to seconds** for objective function evaluation on personal computer

Precomputations

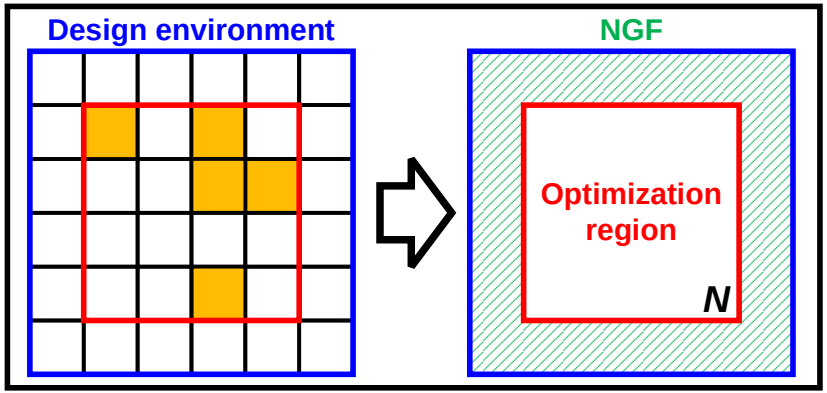

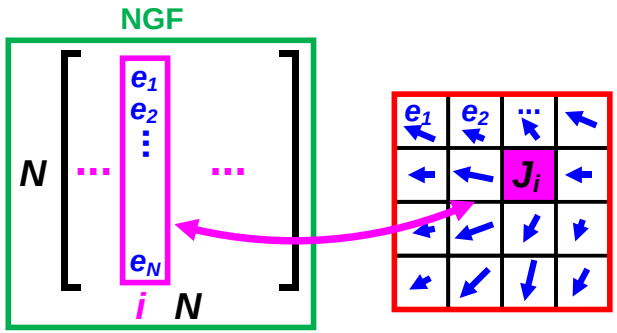

- NGF is *precomputed* once for the design environment and can be used for any number of subsequent optimizations
- Need to solve system for all $J_x^{i,j}$ and $J_y^{i,j}$ source excitations in design region and record collocated tangential $E_x^{i,j}$ and $E_y^{i,j}$ fields and EH_{obj} fields needed for computing objective function at each frequency of interest.

Optimization with NGF

$$C_n \boldsymbol{j} = [(I - P_n) + PG]\,\boldsymbol{j} = P_n \boldsymbol{e}_{inc}$$

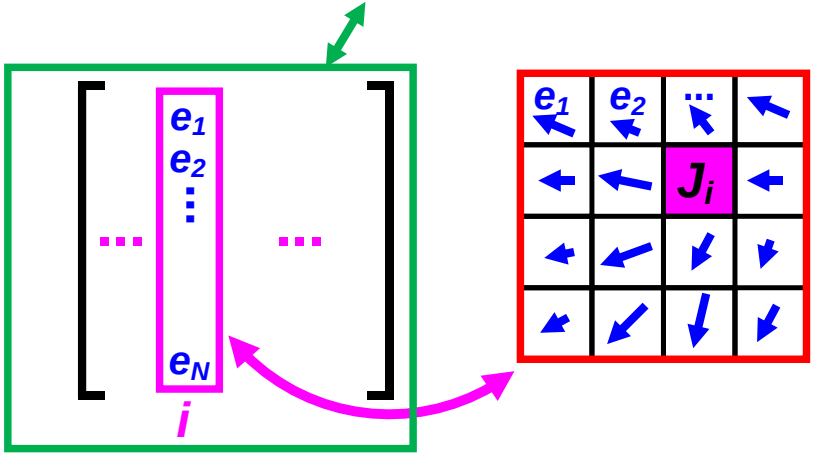

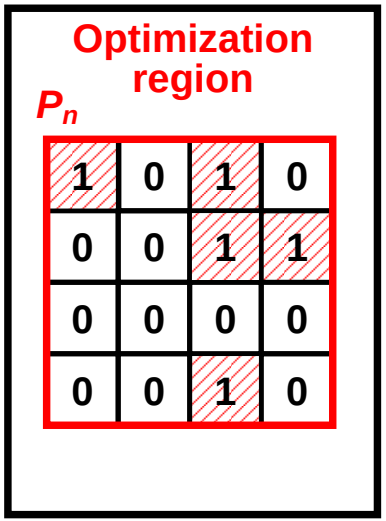

- Represent candidate design with diagonal (0, 1)-matrix P_n
- Solve for C_n^{-1} to find the equivalent currents
- **Direct binary search optimization**: only one tile is changed at once
- Leverage this *low-rank update* to the system to further accelerate evaluation

Example: Switched Beam 5G Antenna Optimization

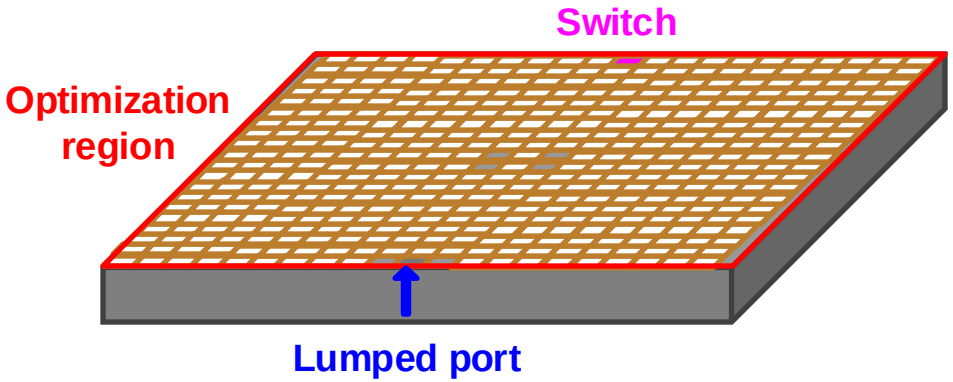

- 0.5mm thick, 10.5 x 10.5mm Rogers RO3035 ($\epsilon_r = 3.5$) dielectric substrate with metal ground plane.
- 50-ohm lumped port at edge and RF switch on other side for switching antenna beam.
- 21x20 tiles on surface (can either be empty or set to metal).

Inverse Design Goals:

- Better than -10dB S11 input matching
- 2) When switch is **ON:** Maximize gain at $\theta, \phi = 45^o, 270^o$ and minimize at $\theta, \phi = 45^o, 90^o$.
- 3) When switch is **OFF:** Minimize gain at $\theta, \phi = 45^o, 270^o$ and maximize at $\theta, \phi = 45^o, 90^o$.

Results (Switch ON)

Switch ON: 1.3GHz impedance bandwidth centered at 30GHz and 11.4 directional gain at $\theta, \phi = 45^o, 270^o$

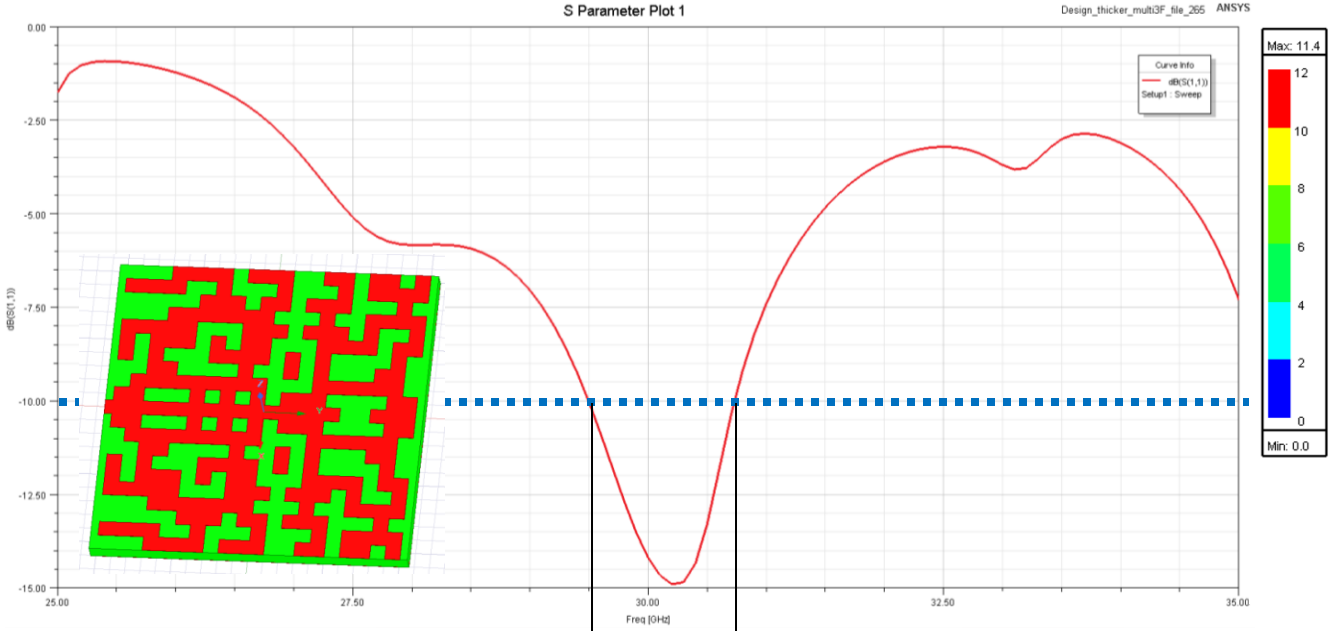

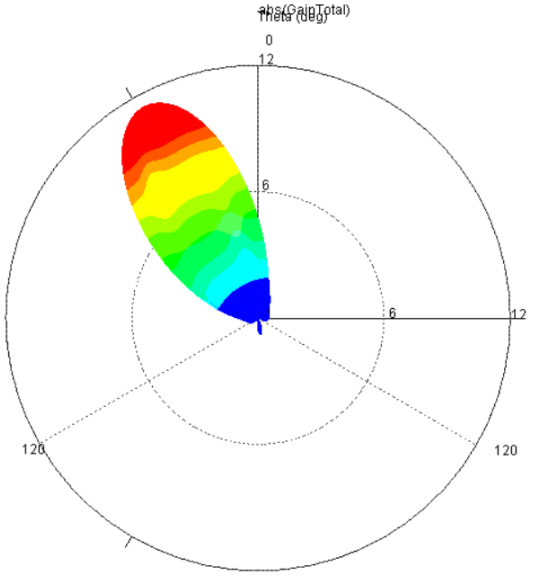

29.5GHz 30.8GHz

Results (Switch OFF)

Switch OFF: 2.2GHz impedance bandwidth and 7.2 directional gain at $\theta, \phi = 45^o, 90^o$

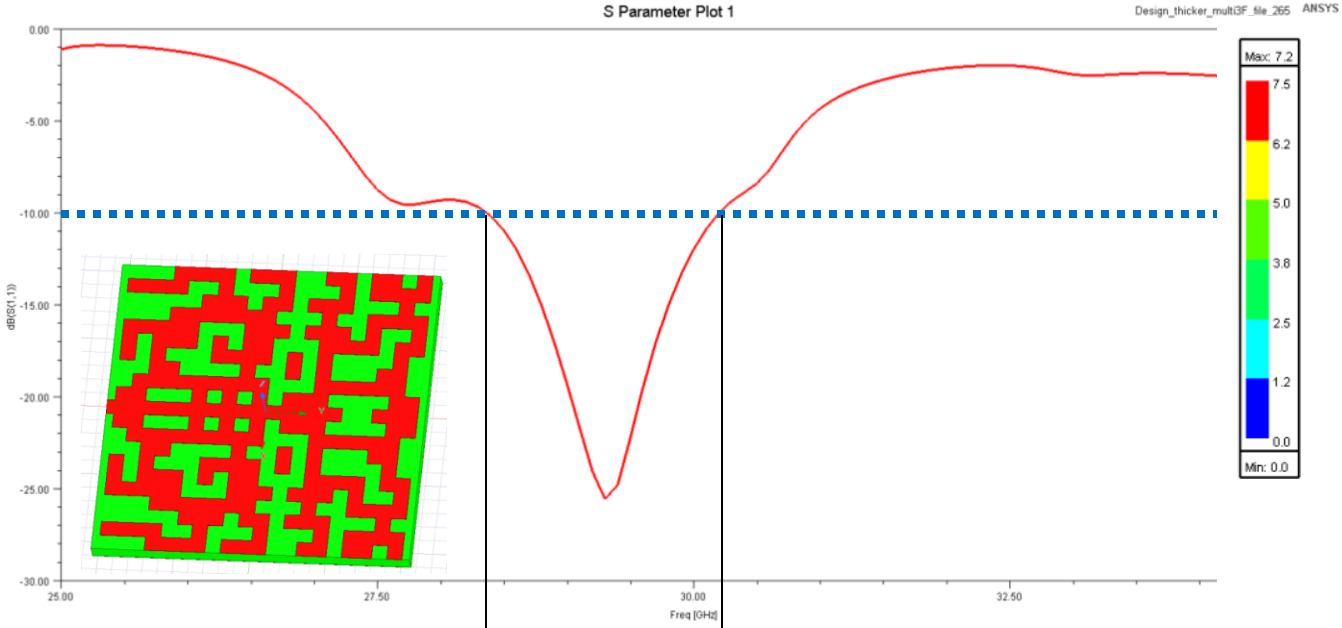

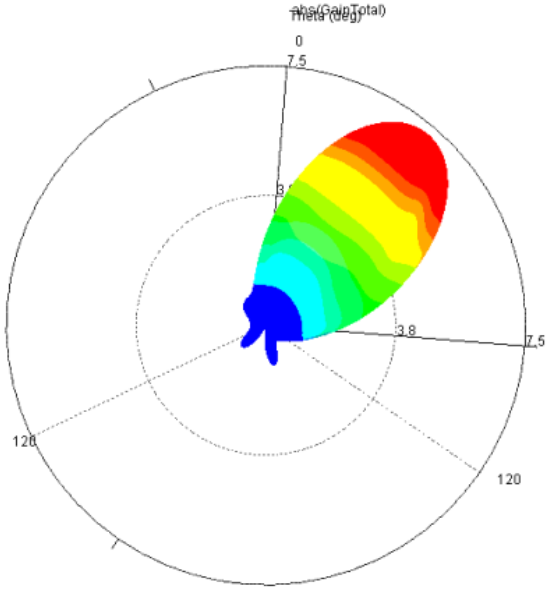

28.4GHz 30.2GHz

Experimental Demonstration

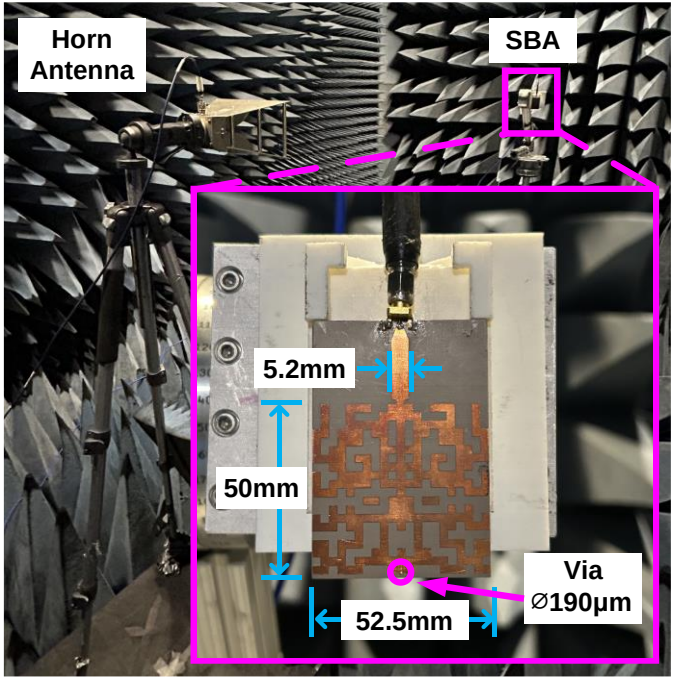

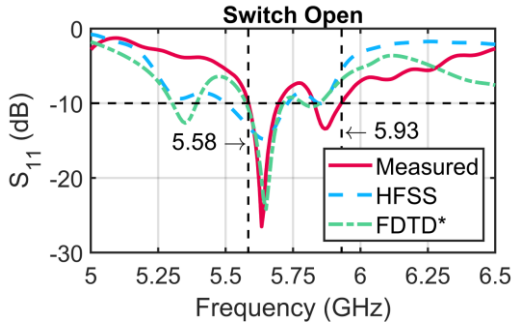

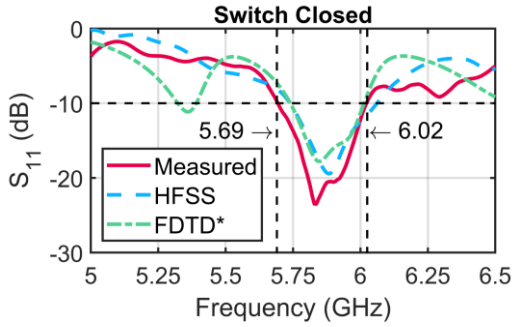

* Simulated without connector

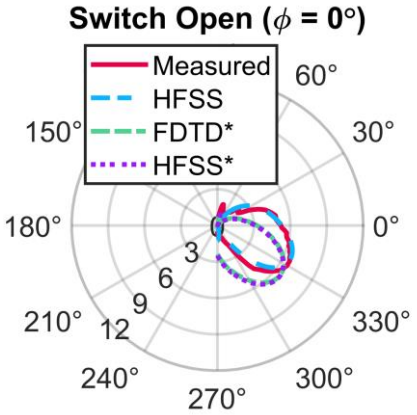

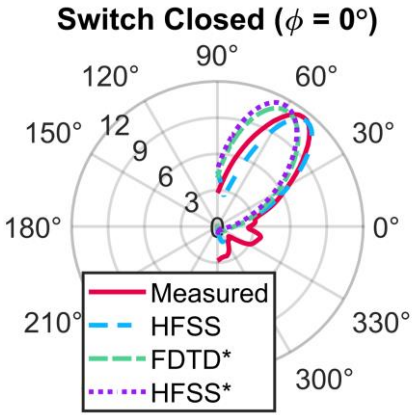

- Scaled-up version with center frequency ~5.7 GHz
- Excellent agreement with simulation results

Experimental Demonstration

Timings

Precomputation:
From 7.6 hr (FDTD) to 14 min (Sparse direct solver)

Optimization:
2.1 hr (3s × 2500)

Speedup: 260x

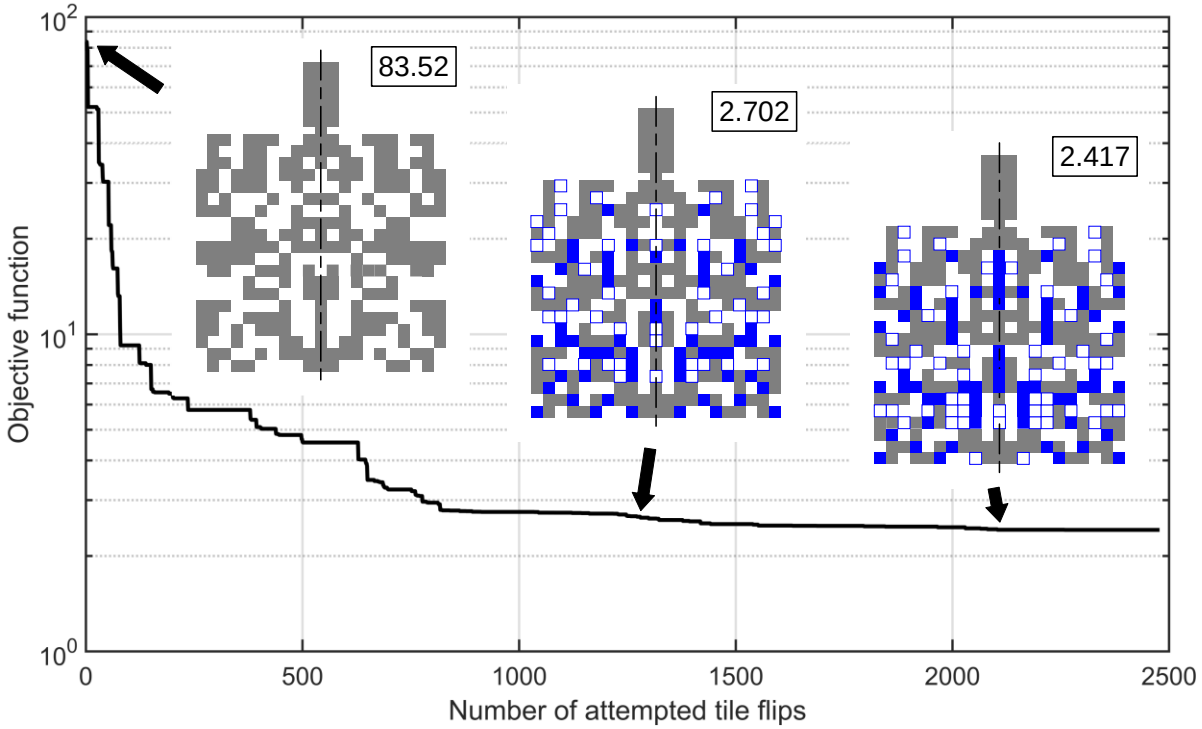

Example: Substrate-Integrated Waveguide Coupler

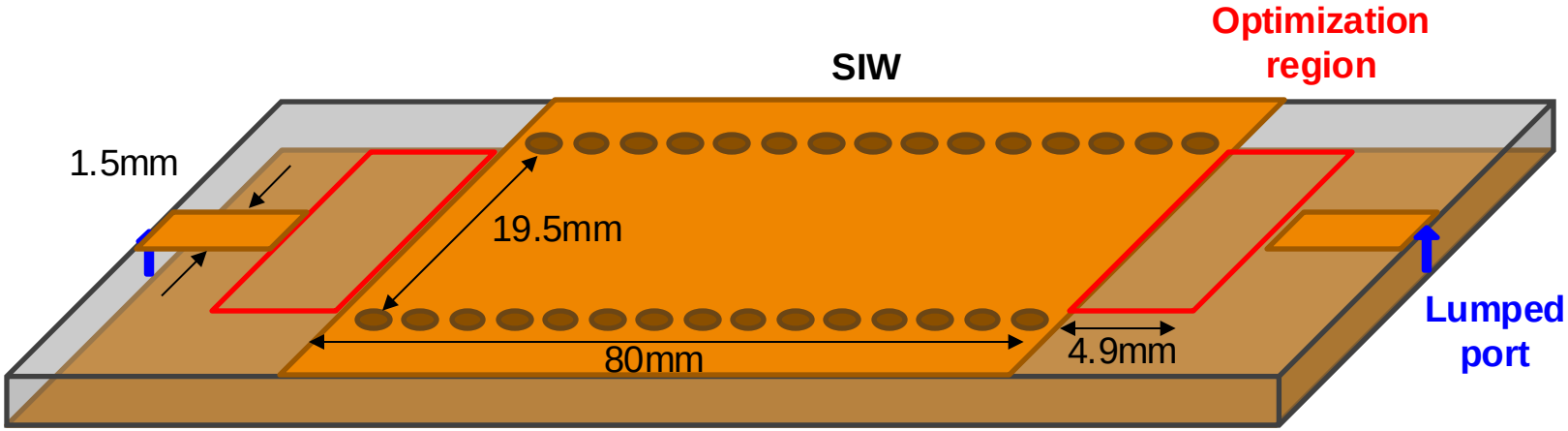

- 0.5mm thick Rogers RT/duroid 5880 ($\epsilon_r = 2.2$) dielectric substrate with metal ground plane.
- 50-ohm lumped port at microstrip feeds
- 52x13 tiles on each transition, identical

Inverse Design Goals:

- 1) Maximum -10dB S11 bandwidth
- 2) Maximize S21

Results and Experimental Demonstration

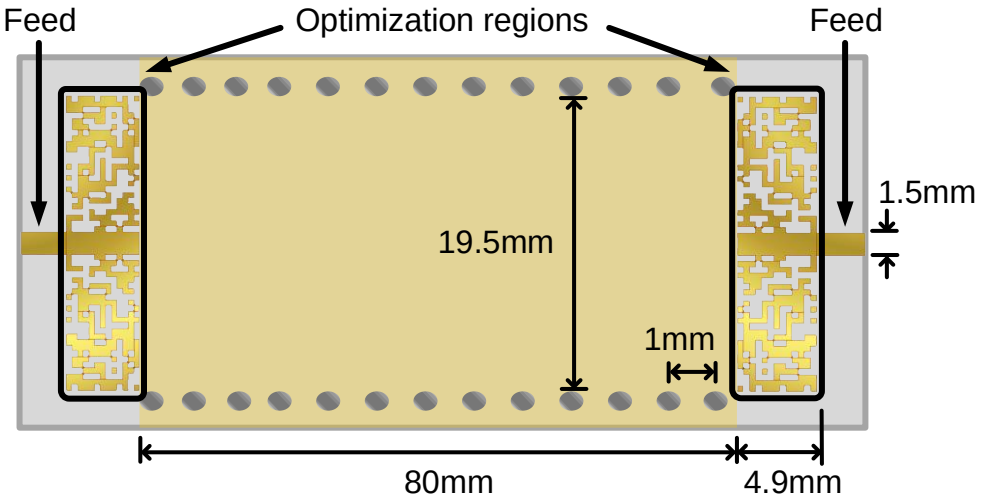

- Objective Function: $f_n = \left(1 - S_{21,n}\right)^2$

- Multi-frequency optimization: Minimize $f_{obj} = \frac{1}{\sum_{n=1}^{N} \frac{1}{f_n}}$

Results and Experimental Demonstration

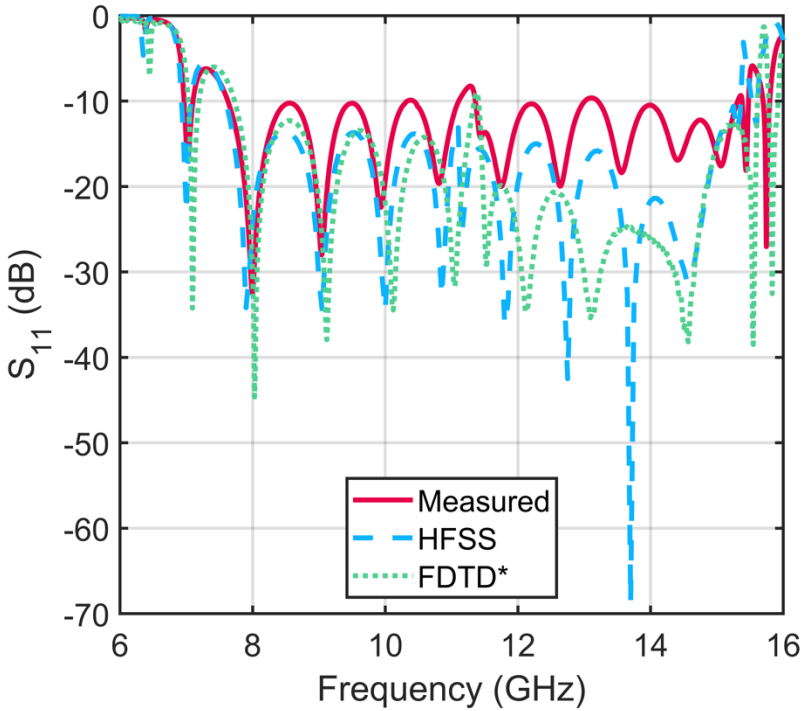

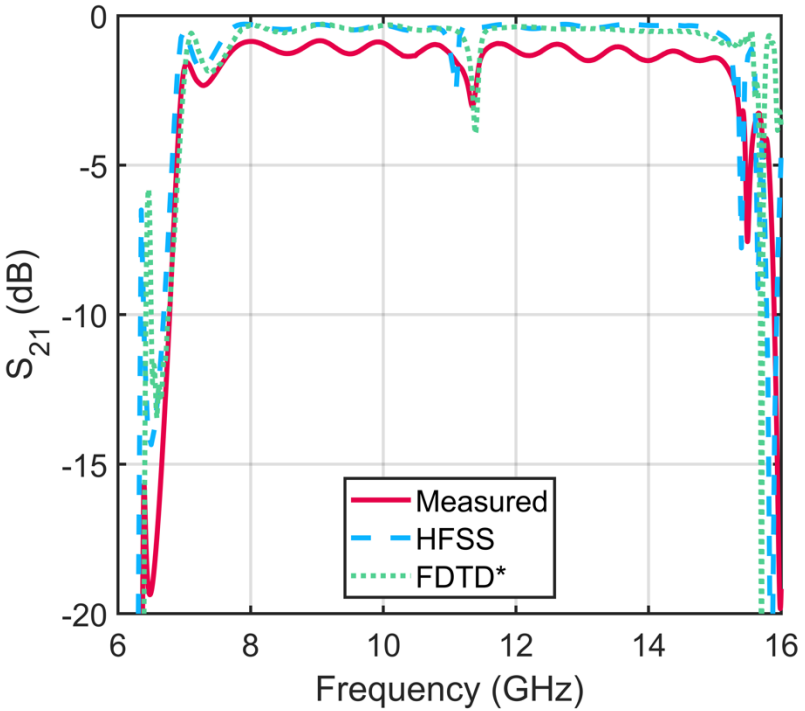

- 10dB bandwidth: 7.7 GHz

* Simulated without connectors

Experimental Demonstration

Timings

Precomputation:
From 12.5 hr (FDTD)
to 30 min (APF)

Optimization:
67min (5s × 880)

Speedup: 470x

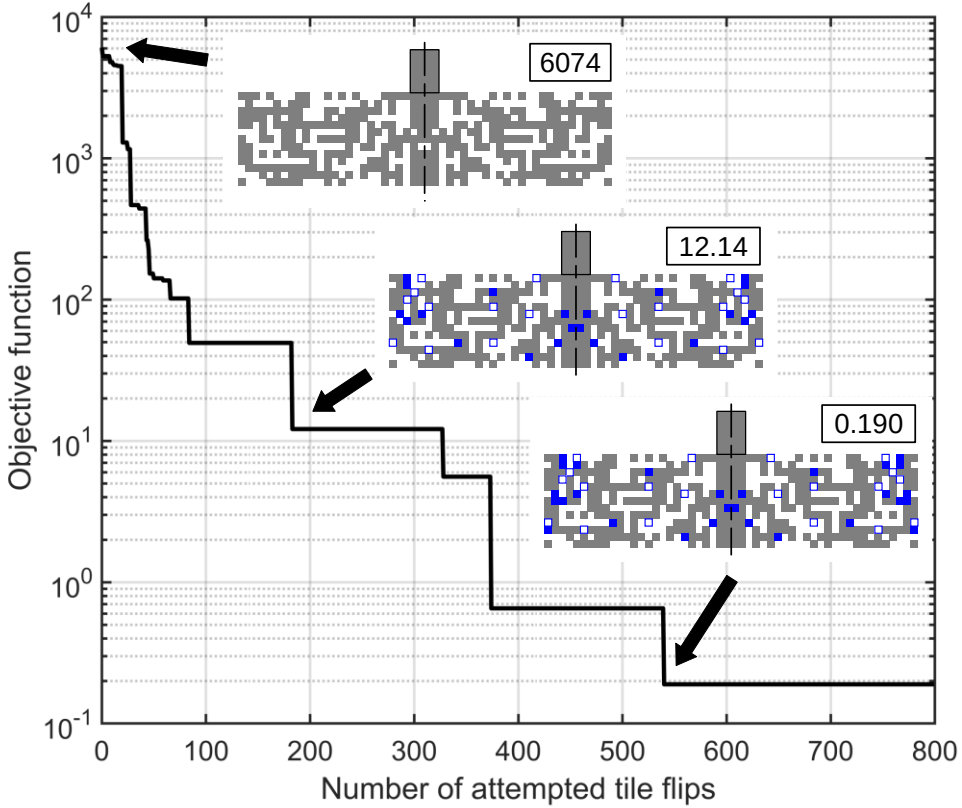

Extension to dielectrics: Nanophotonic Applications

- PNGF can be used just as effectively to represent dielectric materials as equivalent polarization densities to accelerate nanophotonic inverse design problems:

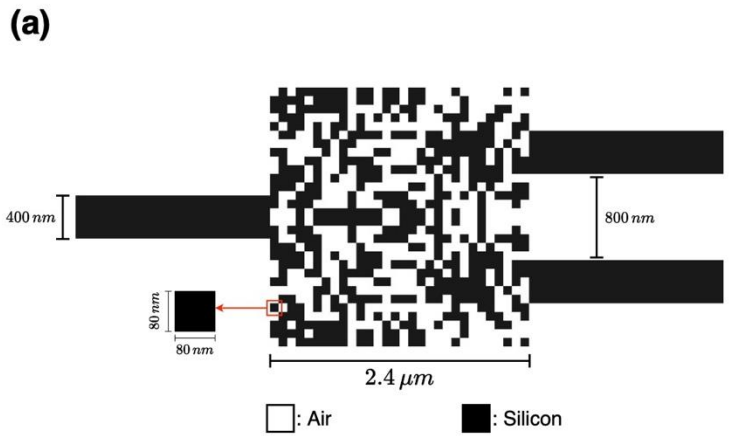

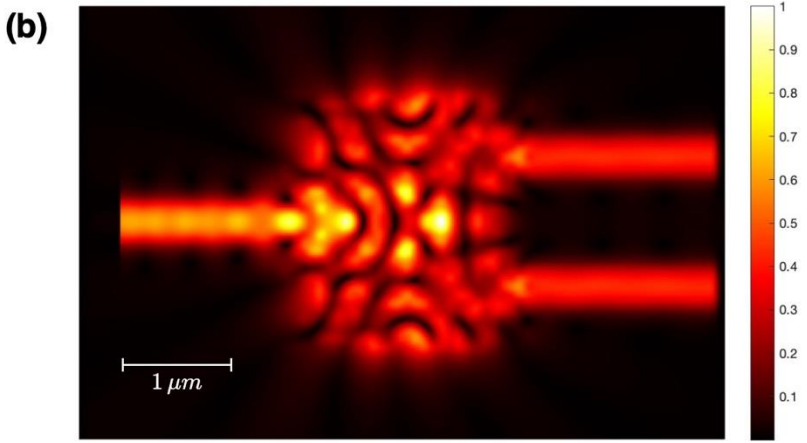

Wang, J. and **Sideris, C.** "Ultra-fast Simulation and Optimization of Nanophotonic Devices using Precomputed Numerical Green's Functions". In preparation.

99.4% efficient 1:2 silicon power splitter

10 seconds to design on laptop computer (3461 flips required to converge)

400x faster than FDFD

Extension to dielectrics: Nanophotonic Applications

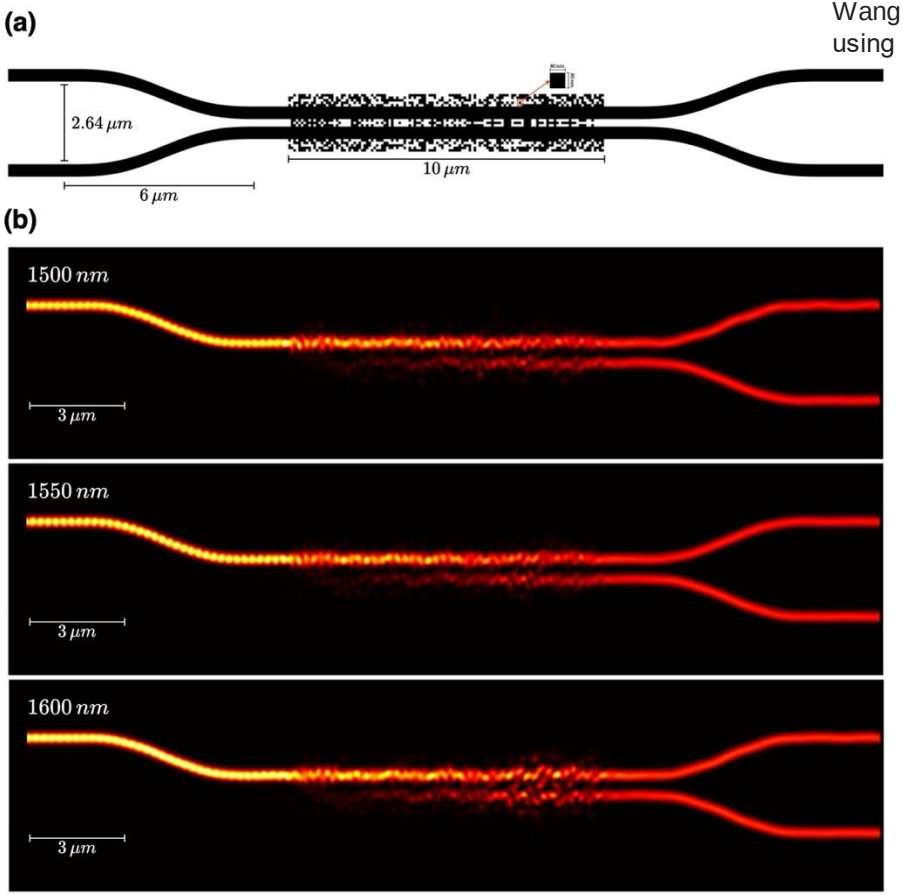

Wang, J. and **Sideris, C.** "Ultra-fast Simulation and Optimization of Nanophotonic Devices using Precomputed Numerical Green's Functions". In preparation.

97.5% transmission broadband symmetric directional coupler with 100nm bandwidth

6 minutes to design on laptop computer (required 10,118 tile flips to converge)

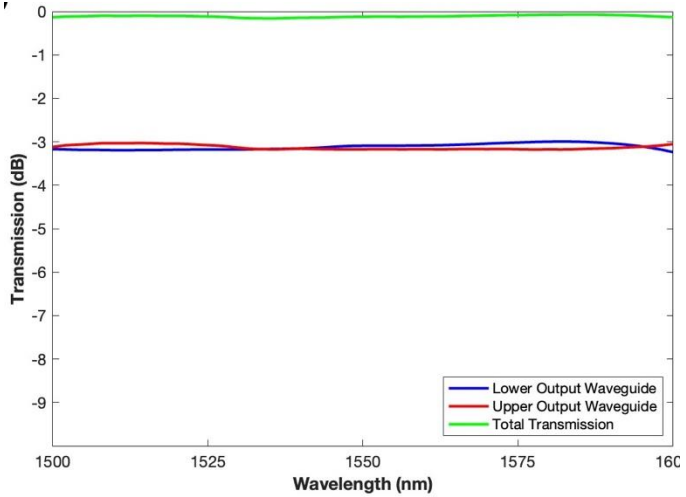

Conclusions and Future Work

- **Multi-level IFGF** for 3D Maxwell: >50x speedup due to O(N log N) vs. O(N^2)

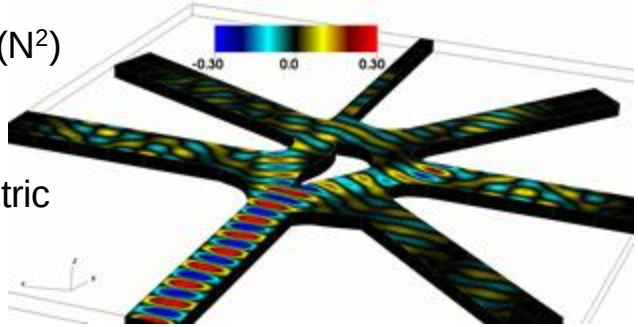

- Corner Regularized Combined Field Integral Equations (**CR-CFIE**) for achieving high-order convergence for scattering from objects with geometric singularities

- **Generalized PNGF** for ultra-fast inverse design of metallic and dielectric structures

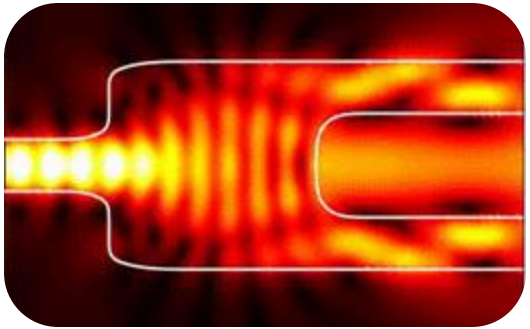

Next Steps:

- Implement multi-level IFGF implementation on GPU to achieve faster performance and O(N log N) time complexity.

- Extend the CR-CFIE method to 3D Maxwell problems.

- Extend the PNGF method for inverse designing 3D nanophotonic devices.

Publications

- Hu, J., Garza, E., and **Sideris, C.** "A Chebyshev-based high-order-accurate integral equation solver for Maxwell's equations." *IEEE Transactions on Antennas and Propagation* 69.9 (2021): 5790-5800.
- Garza, E., Hu, J., and **Sideris, C.** "High-order Chebyshev-based Nyström Methods for Electromagnetics." *2021 International Applied Computational Electromagnetics Society Symposium (ACES)*. IEEE, 2021.
- **Sideris, C.**, Khachaturian, A., White, A., Bruno, O. P., Hajimiri, A., "Foundry-Fabricated Grating Coupler Demultiplexer Inverse-Designed via Fast Integral Methods." Nature Communications Physics, 2022.
- Hu, J., Sever, E., Babazadeh, O., Gholami, R., Okhmatovski, V., and **Sideris, C.** "H-Matrix Accelerated Direct Matrix Solver using Chebyshev-based Nyström Boundary Integral Equation Method". *Presented at IEEE International Microwave Symposium 2022*
- Garza, E., **Sideris, C.**, Bruno, O.P. "A boundary integral method for 3D nonuniform dielectric waveguide problems via the windowed Green function." *IEEE Transactions on Antennas and Propagation (2023).*
- Hu, J. and **Sideris, C.** "A High-Order-Accurate 3D Surface Integral Equation Solver for Uniaxial Anisotropic Media". *IEEE Transactions on Antennas and Propagation* (2023).
- Garza, E. and **Sideris, C.** "Fast Inverse Design of 3D Nanophotonic Devices Using Boundary Integral Methods."*ACS Photonics* (2022).
- Zheng, Y. and **Sideris, C.** "Ultra-fast Simulation and Inverse Design of Metallic Antennas". IEEE International Microwave Symposium (2023).
- Aslanyan, D. and **Sideris, C**. "An Adaptive Integration Technique for the Chebyshev-based Boundary Integral Equation Method." ACES 2023.
- Babazadeh, O., Sever, E., Gholami, R., Jeffrey, I., **Sideris, C.**, and Okhmatovski, V. "Towards Fast Error-Controllable Solution of CFIE on PEC Targets with H-matrix Accelerated Locally Corrected Nystrom Method" URSI EMTS 2023.
- Aslanyan, D., Hu, J., and **Sideris, C.** "Nanophotonic Simulation and Inverse Design using Fast High-order Chebyshev-based Nyström Methods". International Conference on Electromagnetics in Advanced Applications (ICEAA) 2023.
- Huang, J.-Y., Molisch, A.F., **Sideris, C**. "Concurrent Dual Polarization Dielectric Waveguide Interconnect using Inverse Designed Dual-Mode Surface Antenna Launcher". IEEE International Symposium on Antennas and Proapgation (2023).
- Hu, J. and **Sideris, C.** "Unidirectional Waveguide Mode Launching for Boundary Integral Methods." In preparation.
- Hu, J. and **Sideris, C.** "A High-order Nyström-based Scheme Explictly Enforcing Surface Density Continuity for the Electric Field Integral Equation". IEEE AWPL 2024.
- Paul, J. and **Sideris, C.** "Accelerated 3D Maxwell Integral Equation Solver Using the Interpolated Factored Green Function Method" In revision (IEEE TAP). Available on Arxiv.
- **Sideris, C.,** Aslanyan, D., and Bruno, O. "High-order-accurate Solution of Scattering Integral Equations with Unbounded Solutions at Corners". In preparation.
- Zheng, Y., Elsawaf, M., Hung, J., Lin, H.-C., Hsu, C.W., **Sideris, C.** ""Ultra-fast Inverse Design of Radio-Frequency Electromagnetic Devices". In preparation.
- Wang, J. and **Sideris, C.** "Ultra-fast Simulation and Optimization of Nanophotonic Devices using Precomputed Numerical Green's Functions". In preparation.